New approach to evaluate the angular transmission of the in-flight separator FRS at GSI

Jorge Pereira Conca

November 1999

Contents

Hoy en día, los espectrómetros magnéticos en vuelo constituyen una herramienta indispensable muy utilizada en experimentos de Física de Altas y Bajas energías. Gracias a su alta resolución en momento, estos dispositivos permiten el estudio detallado de los diversos mecanismos de reacción conocidos. Por otro lado, constituyen una excelente fuente de haces radioactivos producidos a traves de reacciones de fragmentación de proyectiles. El Separador de FRagmentos FRS, en el GSI, constituye un buen ejemplo de este tipo de espectrómetros. Su uso más reciente ha sido el de la investigación de reacciones de espalación en cinemática inversa. Este tipo de reacciones no solo tienen un gran interés en Astrofísica sino que constituyen una excelente fuente de neutrones para la transmutación de resíduos nucleares.

El estudio de la distribución isotópica de los resíduos producidos en reacciones de espalación resulta decisivo para cualquiera de las aplicaciones mencionadas. En el caso de la Astrofísica Nuclear, estos resíduos juegan un papel decisivo en el análisis de las abundancias isotópicas en el Sistema Solar. Por otro lado, las altas intensidades de protones ($\sim$ 100 mA) utilizadas por las fuentes de espalación, requieren un análisis detallado de los resíduos producidos (la mayor parte de ellos radioactivos). Estos resíduos determinarán la radioactividad final del blanco. Además, el estudio de sus propiedades cinemáticas permitirá la valoración del daño causado por radiación a la estructura que constituye la fuente de espalación y sus alrededores.

Desde un punto de vista experimental, la mayor parte de los estudios sobre resíduos producidos en reacciones de espalación han sido realizados con métodos radioquímicos. Esta técnica se basa en la identificación de núcleos a través de su desexcitación por emisión de fotones. La mayor limitación de este método es que los fotones medidos pueden también ser emitidos después de decaimientos β dificultando la medida de la sección eficaz del núcleo estudiado. Este problema se puede evitar estudiando la reacción en cinemática inversa, lo cual facilita el estudio de los fragmentos pesado emitidos en una dirección próxima a la del haz incidente. La mayor parte de estos núcleos pueden ser transmitidos a través de un separador magnético en vuelo, permitiendo su medida y posterior identificación.

El estudio de la producción de núcleos a través de reacciones de espalación

como posibles fuentes de neutrones utilizadas en la transmutación de resíduos nucleares requiere medidas precisas con incertidumbres menores a un 10%. Para alcanzar tal grado de precisión, todos los factores a tener en cuenta a la hora de determinar las secciones eficaces de producción deben ser conocidos con gran exactitud. Entre estos factores se incluyen no solo la intensidad del haz primario o la eficiencia de los detectores sino también la transmisión de los núcleos producidos a través del separador en vuelo. De hecho, este factor cobra una importancia decisiva en reacciones de fisión, donde la tasa de núcleos transmitidos es extremadamente baja en comparación con la tasa de producción.

El presente trabajo se centra en el estudio de la transmisión de partículas cargadas a través de espectrómetros magnéticos, considerando tanto las características ópticas del dispositivo como la cinemática debida a los distintos mecanismos de reacción. A través de simulaciones Monte-Carlo, hemos podido realizar un estudio detallado de la transmisión angular para separadores en vuelo. El objetivo de este trabajo ha sido el análisis de los diferentes parámetros que intervienen en dicha transmisión angular. Finalmente, proponemos un nuevo método que simplifica extremadamente los tediosos cálculos Monte-Carlo.

El trabajo se estructura en varios capítulos:

- En el primer capítulo se presenta, a modo introductorio varias técnicas utilizados en la identificación de masas nucleares. Al comparar las resoluciones en masa alcanzadas con cada una de ellas se concluye que los espectrómetros magnéticos en combinación con medidas del tiempo de vuelo constituyen el método ideal para la identificación de núcleos pesados. A continuación se ofrece una descripción detallada del separador en vuelo FRS utilizado en el GSI. Como se verá, dicho dispositivo permite tanto la seleción de núcleos a analizar, como su identificación en masa y carga.

- El segundo capítulo se centra en la problemática de la transmisión a través de separadores magnéticos en vuelo. Esta transmisión viene dada por las aceptancias en ángulo y momento del sistema así como por la cinemática de los núcleos transmitidos. Ambos factores son descritos en detalle. Finalmente, como se verá, las aceptancias dependen de las características ópticas del separador y de sus dimensiones.

- En el tercer capítulo presentamos los resultados del análisis de dos experimentos realizados en el FRS. El objetivo de estos análisis fue el estudio cualitativo de la transmisión de núcleos producidos en reacciones de fisión a través del FRS. Los resultados muestran como este es-

pectrómetro corta las ditribuciones de velocidad y ángulo de los núcleos producidos.

- El capítulo cuarto es el núcleo de esta Tesina. En él se describen detalladamente los cálculos de la transmisión angular a través del FRS realizados mediante un nuevo método. Este método se basa en el cálculo, a través de simulaciónes Monte Carlo de la aceptancia angular del FRS en función de variables globales que describen las trayectorias seguidas por los núcleos. Posteriormente, se explica cómo determinar analitícamente la transmisión para cualquier núcleo considerando, tanto la aceptancia angular calculada como la cinemática de los núcleos transmitidos debida al mecanismo de reacción.

  Este método ofrece un máximo ahorro del tiempo invertido en los cálculos Monte-Carlo, así como una alta precisión en los resultados obtenidos.

- Finalmente, en el capítulo quinto se da una evaluación del trabajo realizado, así como una discusión de los resultados obtenidos.

Introduction

In-flight separators are nowadays an extensively used tool in experimental nuclear physics. Due to their high momentum resolution, these spectrometers allow detailed investigation of the nuclear reaction mechanisms. They are also a key element in the production of radioactive nuclear beams by projectile fragmentation reactions. Recently, the FRagment Separator FRS [1] at GSI, Darmstadt, has been used to investigate spallation reactions in inverse kinematic. These reactions have a large interest in nuclear astrophysics, but they are also considered as an optimal neutron source for material-science investigation [2] or for the transmutation of nuclear waste [3, 4].

The investigation of the isotopic distribution of the spallation residues is decisive for any of the mentioned applications. In the case of nuclear astrophysics, these residues play an important role in the observed solar-system abundances. The high proton-beam intensities planned to be used in the spallation sources ($\sim$ 100 mA) lead to an important inventory of spallation residues (most of them radioactives) which will determine the final radioactivity in the target. In addition, the investigation of the kinematical properties of these residues will help to determine the radiation damage in the structural materials which constitute the spallations source and its surroundings.

From an experimental point of view, the residue production in the spallation reactions has mainly been investigated by radiochemical methods. This technique is based on the identification of the produced residues by their gamma decay. The main limitation of this method is that the measured photons can also be emitted after β-decay and therefore mainly cumulative yields are determined. In order to overcome this limitation, an alternative method has recently been proposed to be used in the new high-energy facilities at GSI. This method consists in the study of the reaction in inverse kinematic in which all heavy residues are emitted on forward direction. Finally, a high-resolution in-flight separator will allow the isotopical identification of all these residues.

The study of the residue production in spallation reactions in neutron sources used for the transmutation of nuclear waste requires high-accurate

measurements with uncertainties lower than 10%. To achieve such precision, all the parameters entering into the cross-section determinations must be known very accurately. This includes not only the primary-beam intensity and the efficiency of the detectors but also the transmission of the produced nuclei passing through magnetic spectrometer. This last factor is particularly important in the analysis of fission reactions, since only a small part of the fission fragments is transmitted.

The present work is devoted to the study of the transmission of charged particles through a magnetic spectrometer, taking into account the ion-optic properties of the apparatus and the kinematics of the reaction residues to be investigated. By using Monte-Carlo ion-optical calculations we have performed a comprehensive study of the angular transmission in zero-degree spectrometers. The aim was to get a systematic view on the parameters which determine this angular transmission. From this work, we conclude that the transmission can be described as a function of few parameters with analytical expressions which simplifies the arduous Monte-Carlo calculations.

The work is organised in the following way:

- In the two first chapters we describe the method used for masses identification with magnetic spectrometers, and we introduce the problematic of the losses due to the limited transmission through the spectrometer.
- In the third chapter we present the results of two different experiments analysed, which illustrate the problematic of the transmission.
- The fourth chapter is devoted to the Monte-Carlo code developed to simulate the transmission through a spectrometer. The results of the simulation show that the transmission can be described in terms of a few factors, and we present an analytic description to simplify the calculation of the transmission.
- This work concludes with an evaluation of the results obtained.

Chapter 1

Isotopic identification with magnetic spectrometers

The determination of the production cross-sections of the isotopes produced in heavy-ion reactions requires a high resolution detection system to determine mass and atomic number. At relativistic energies, the atomic number can easily be deduced from energy-loss measurements, to determine the mass, however, more complicated detection systems are required.

In order to distinguish two neighbouring heavy nuclei, a resolution better than $\Delta A/A \simeq 0.25/250 = 10^{-3}$ is required.

In this chapter, we will discuss different methods for the identification of nuclear masses. The comparison of these methods will illustrate the main advantages of the magnetic identification.

In the second part of the chapter, we will describe the principles of the magnetic identification in detail. For that purpose, we will use the FRagment Separator FRS at GSI as an example. As we will see, the complexity of such devices justifies the efforts necessary to determine the transmission of charged particles.

1.1 Methods for mass identification

Different techniques can be applied to identify the masses of nuclei produced in heavy-ion reactions; they are based on the measurement of different quantities related to the nuclear mass:

The measurement of the kinetic energy and velocity of a fragment can provide the identification of its mass, since these variables are related through the equation:

$$E = \frac{1}{2} A v^2 \tag{1.1}$$

The kinetic energy can be measured with scintillators, semiconductors or gas detectors whereas the velocity is obtained from the time-of-flight (ToF) measured between two detectors separated by a distance d:

$$ToF = \frac{d}{v} \tag{1.2}$$

In order to measure the kinetic energy, the nucleus must be stopped by the detector. If we want to measure the kinetic energy of a ^{208}Pb nucleus with a 50 cm length gas detector filled with ^{40}Ar at atmospheric pressure, the maximum energy of the nucleus to be stopped is about 40 A MeV. Therefore, this method can only be applied at low energies.

If we calculate the mass resolution reached with this method using the values reported in table 1.1, we will conclude that this method is only valid for light masses, namely $A \leq 25$.

$$\frac{\Delta A}{A} = \sqrt{\left(\frac{\Delta E}{E}\right)^2 + 2\left(\frac{\Delta ToF}{ToF}\right)^2} \simeq 10^{-2} \tag{1.3}$$

A second method consists in measuring both the energy loss and the kinetic energy of a nucleus with telescope detectors. The Bethe-Bloch theory predicts that this energy-loss can be roughly calculated with the following equation:

$$\Delta E \sim \frac{A \cdot Z^2}{E} \tag{1.4}$$

Therefore, if we know the energy-loss and the kinetic energy it is possible to determine the masses. Once again, we can calculate the mass resolution obtained with this method using the values of table 1.1:

$$\frac{\Delta A}{A} = \sqrt{\left(\frac{\Delta E}{E}\right)^2 + \left(\frac{\Delta(\Delta E)}{(\Delta E)}\right)^2} \simeq 10^{-2} \tag{1.5}$$

The result shows that the resolution of this method is only acceptable for masses in the range of $A \leq 25$. In addition, the measurement of the kinetic energy, is also limited to low kinetic energies (E <50 A MeV).

The third method uses magnetic spectrometers. This technique is based on the measurement of the magnetic rigidity and velocity of a nucleus traversing a uniform magnetic field:

$$B\rho = \frac{1}{e}\frac{A}{Z}\beta\gamma c \tag{1.6}$$

where B is the magnetic field, ρ is the curvature radius of the trajectory followed by the nucleus inside the magnet, e is the electron charge, A and

Z are the mass and charge of the nucleus c is the velocity of light and $\beta\gamma$ the relativistic factor. The curvature radius is measured by position-sensitive detectors whereas $\beta\gamma$ is obtained from the time-of-flight and the flight path of the traversing nucleus d. If these quantities are known, the mass of an isotope can be evaluated. The mass resolution achievable by this method can be calculated using the following equation:

$$\frac{\Delta A}{A} = \sqrt{\left(\frac{\Delta B\rho}{B\rho}\right)^2 + \frac{ToF^4c^4}{ToF^2c^2 - d^2} \cdot \frac{1}{d^2}\left(\frac{\Delta ToF}{ToF}\right)^2} \tag{1.7}$$

where d is the flight path.

Let us consider as an example a ^{208}Pb nucleus accelerated up to 800 A MeV. If we assume a flight path of d =4 m, the time-of-flight of the nucleus will be ToF =174 ns. Using these values and those reported in table 1.1, the mass resolution calculated from equation 1.7 is about 10^{-3}. Therefore, this method provides the resolution needed to identify heavy masses and can also be applied at high energies.

Variable	Detector	Resolution	Range
E	semiconductor	10^{-3}	paths < 1cm
	scintillator	10^{-2}	E > 1 A MeV
	gas	10^{-2}	paths < 1m.atm
ΔE	semiconductor scintillator gas	10^{-2}	E > 1 A MeV
$B\rho$	spectrometer	$10^{-3} - 10^{-5}$	E > 1 A keV
ToF	scintillators	$\Delta t/t$ depends on d	E > 1 A MeV
	gas	$10^{-2}-$	
	semiconductors	-10^{-4}	

Table 1.1: *Resolutions obtained with different detectors. The last column shows the typical operation ranges of each detectors.*

1.2 Isotope identification with magnetic spectrometers

As already pointed out in the previous section, the mass of a nucleus can be identified from the measurements of the magnetic rigidity of this nucleus passing through an uniform magnetic field. Dipole magnets are used to bend the trajectory of charging particles according to their magnetic rigidity. Therefore, one could isotopically identify the reaction residues from their deflection in angle. However, this is a rough simplification of the problem. Three different factors contribute to complicate the design of magnetic spectrometers: the resolution necessary to identify masses, the optimisation of the transmission and the separation of the nuclear residues.

Resolution

Two factors must be considered to estimate the intrinsic resolution achieved with a dipole magnet: the dispersion of the magnet and the magnification in the deflection-direction, both concepts are explained in appendix A. The resolution can be enhanced either by increasing the dispersion or by reducing the magnification, which means a much more complex design of the magnetic system. For instance, the dispersion raises with increasing both the length of the dipole and the curvature radius. On the other hand, the magnification can be reduced by adding quadrupoles to the dipole magnet in order to modify the ion-optical conditions of the image plane behind the magnetic system.

Transmission

Quadrupoles in front of the dipole must be included in order to optimise the transmission of the produced nuclei through the magnetic spectrometer. These quadrupoles match the acceptance of the spectrometer and the emittance of the nuclei to be analysed and simultaneously shapes the beam in order to appropriately illuminate the dipole magnets.

Separation

In typical heavy-ion reaction, a huge amount of reaction residues are produced. In principle, we are only interested in a subset of these products. Therefore, one should be able to select the products of interest. In-flight separators provide the required selection criteria. These devices are powerful

tools which allow both the selection of nuclei to be analysed and the measurement of their masses. A detailed description of them can be found in references [5, 6]. The design of in-flight separators is much more complicated than a simple dipole. For instance, they combine several dipoles to achieve the separation criteria. In addition, quadrupoles and sextupoles are included to optimise the transmission of the separated nuclei as well as to correctly define the image planes.

The FRagment Separator (FRS) at GSI is an example of in-flight separators. The nuclear selection is done by using the momentum-loss achromatic method [7]. The main important characteristics of this device will be explained in the next section.

1.3 The FRagment Separator FRS at GSI

1.3.1 Description of the FRS

The FRS is a zero-degree spectrometer which can also be used as a separator. It consists of two symmetric stages in order to ensure the achromatism of the system, as we will discuss later (section A.3.4).

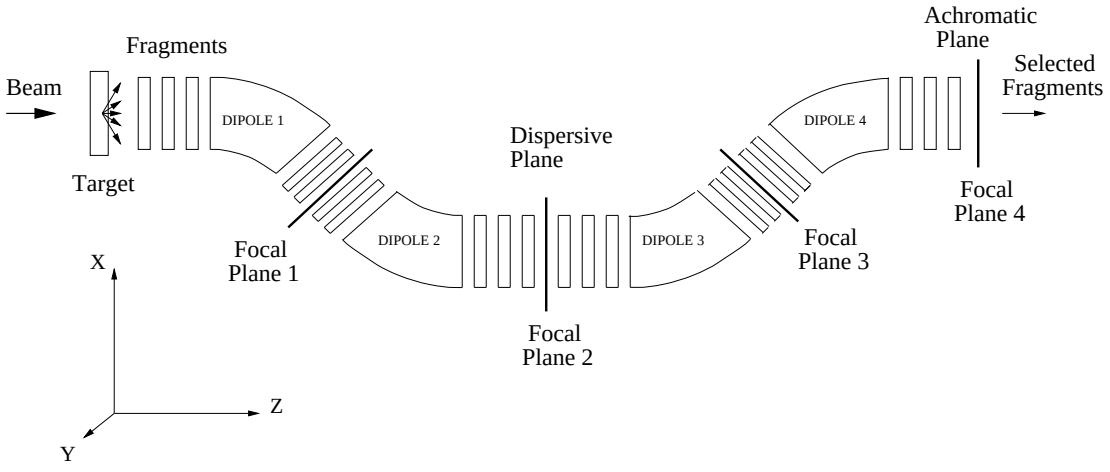

Figure 1.1: *Layout of the FRS at GSI showing the most important magnetic elements. Quadrupoles are placed before and after each dipole to define the ion-optic conditions at each image plane as well as to maximise the transmission through the spectrometer. Sextupoles behind the dipoles are not included in the figure; they correct for high-order aberrations.*

Figure 1.1 shows the two stages of the FRS. Each stage consists of two dipoles and a set of quadrupoles and sextupoles. The four dipoles provide the required magnetic field to bend relativistic heavy ions ($B\rho \simeq 18$ Tm). The quadrupoles in front of the dipoles are adjustable to properly illuminate the entrance of the ions in the bending magnets in order to maximise the transmission. The quadrupoles following the dipole magnets determine the ion-optical conditions at the four image planes. The sextupoles are used to correct second-order aberrations and to avoid the dependencies on momentum of the image plane positions. The physical dimensions of the system (6 m per dipole, 70 m total length) are determined by the magnetic rigidity of the investigated particles (≤ 18 Tm) and the maximum magnetic fields ($B \simeq 1.6$ T) achievable with standard technologies. The design of the separator limits the angular and the magnetic rigidity acceptances to $\Delta B\rho/B\rho \simeq \pm 1.5\%$ and $\Delta\theta \simeq \pm 15$ mrad, respectively. These aspects of the separator will be discussed in detail in the next chapter.

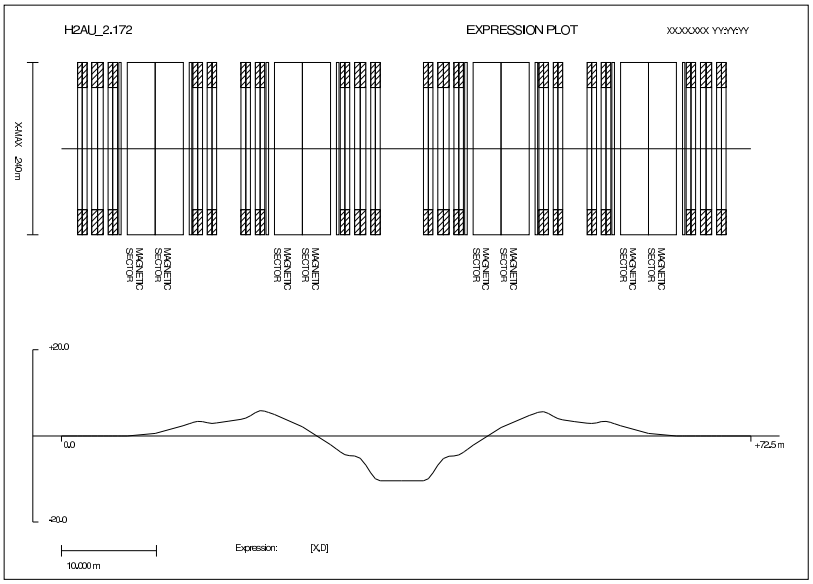

Figure 1.2: *Transversal x-position of a nucleus traversing the FRS with momentum deviation of 1% with respect to that of the nucleus following a central-trajectory. The nucleus traverses the second image plane (the dispersive plane) at a transversal position of x= -6.8 cm demonstrating that the maximum dispersion is reached at this image plane. This dispersion is cancelled by the one of the second stage, so that the overall separator is achromatic.*

In its achromatic configuration, the FRS has two important image planes,

a dispersive one (the second) and an achromatic one (the fourth). Figure 1.2 shows the ion-optical characteristic of the FRS. The figure illustrates the trajectory followed by a particle traversing the FRS with a momentum 1% higher than that of the particle following a central-trajectory (section A.2). It is clearly demonstrated that the maximum dispersion of -6.8 cm/% is reached at the second image plane (the dispersive plane). The dispersions of the first and the second dipoles are cancelled by that of the third and fourth, so that the overall system from the target to the fourth image plane (the achromatic plane) is achromatic (section A.3.4).

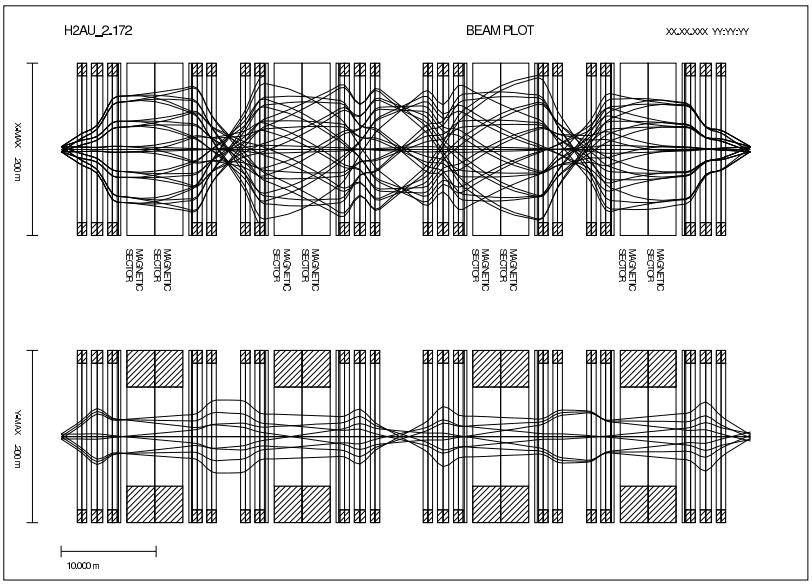

Figure 1.3: *Transversal positions of the trajectory followed by nuclei entering into the FRS with different angles and momenta. Up: transversal x-positions. Down: transversal y-positions. It can be noted that nuclei with a relative momentum deviation equal to zero traverse all the image planes at centred x-positions, while the same condition is only achieved at the dispersive and achromatic image planes for the vertical y-position.*

Figure 1.3 shows the trajectories followed by the nuclei entering into the FRS with different angles and momenta. The dipoles split the trajectories of the nuclei with different values of momentum. Nuclei with momentum deviations of $\pm 1\%$ traverse the second image plane at ± 6.8 cm, while those without momentum deviations and with different angles at the entrance, traverse all the image planes at the same x-position.

For a magnetic spectrometer like the FRS, the magnetic rigidity of the traversing nuclei is directly related to their transversal x-position at the dif-

ferent image planes. This relation can be obtained from the equations describing the trajectory of an ion inside the spectrometer:

Magnetic rigidity determination

The equation of motion of a charged particle passing through the separator can be expressed in terms of the variables describing its trajectory (see appendix A):

$$x(s) = \frac{\partial x}{\partial x'}x' + \frac{\partial x}{\partial \theta'}\theta' + \frac{\partial x}{\partial y'}y' + \frac{\partial x}{\partial \phi'}\phi' + \frac{\partial x}{\partial \delta p'}\delta p' \tag{1.8}$$

where the prime refers to the initial values of the variables.

In this section we will use the notation of Brown [8] (see appendix A). At the image planes, the x-position of the transmitted particles does not depend on their angles:

$$(x \mid \theta') = \frac{\partial x}{\partial \theta'} = 0 \tag{1.9}$$

$$(x \mid \phi') = \frac{\partial x}{\partial \phi'} = 0 \tag{1.10}$$

where θ' is the transversal horizontal angle (in the x-z plane) and ϕ' is the vertical one (in the y-z plane) (see figure A.5). In addition, if the nuclei are supposed to enter into the FRS with central x-positions ($x_0 = 0$), the x-position at the second image plane can be calculated with the following equation:

$$x_2 = (x \mid \delta p)_{02}\delta p_0 \tag{1.11}$$

where $(x \mid \delta p)_{02}$ is the dispersion on x-direction due to momentum deviation. Subscripts 0 and 2 refer to the particle coordinates at the entrance of the FRS and at the second image plane, respectively.

When the charge of the studied particle coincides with that of the reference particle, we can assume that $\delta p = \delta B\rho$. Then, the transversal x-position at the second image plane can be expressed as a function of the deviation in relative magnetic rigidity:

$$x_2 = (x \mid \delta p)_{02}\delta B\rho \tag{1.12}$$

In contrast to x_0, x_2 can take values appreciably different from zero, so that we must include an additional term for calculating the horizontal position at the fourth image plane:

$$x_4 = (x \mid x)_{24}x_2 + (x \mid \delta p)_{24}\delta B\rho \tag{1.13}$$

where the subscript 4 refers to the position at the fourth image plane.

Equations 1.12 and 1.13 show the relation between transversal x-position at the second and fourth image planes and the magnetic rigidity of the nuclei. Therefore, this magnetic rigidity can be determined by measuring the transversal positions of the transmitted particles at these image planes.

1.3.2 Isotope identification with the FRS

To identify the residues produced in heavy-ion reactions, special methods such as those described in section 1.1 are required. As we have mentioned, the use of magnetic spectrometers in combination with velocity measurements, allows the mass determination with high resolution. In this section we will describe how one can determine the mass of nuclei traversing the FRS:

From equation 1.6 one can deduce the mass of a nucleus traversing the FRS:

$$A = \frac{e}{c} \cdot \frac{Z}{\beta\gamma} \cdot B\rho \tag{1.14}$$

Figure 1.4 shows the FRS with the detectors used to measure these quantities.

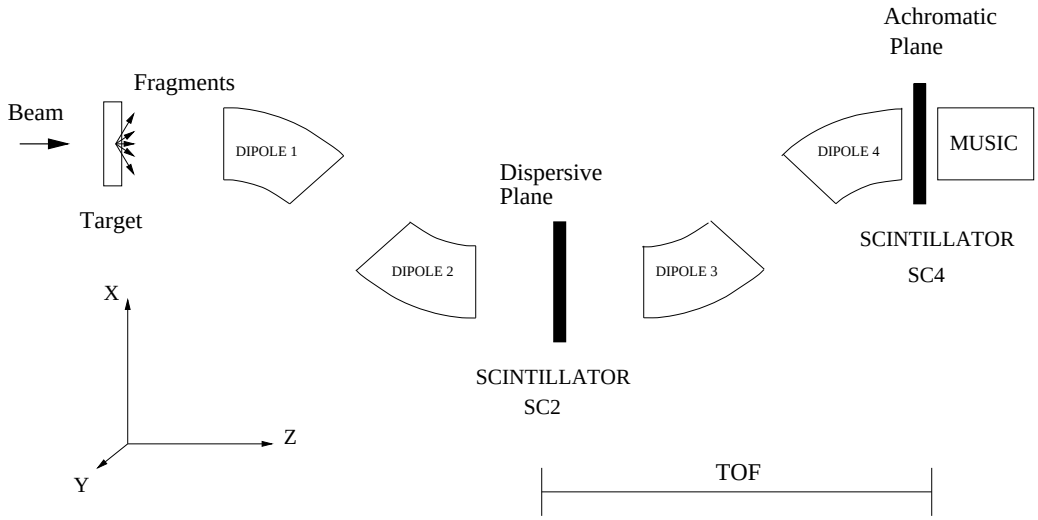

Figure 1.4: *Standard detection set-up used at the FRS for the isotope identification. Transversal x-position of the transmitted nuclei are determined by position-sensitive scintillators placed at the second and fourth image planes (SC2 and SC4). The time-of-flight is measured between these two detectors separated by a distance d=35 m. The nuclear charges are determined from the energy-loss measurements performed by a MUlti-Sample Ionisation Chamber (MUSIC), placed at the exit of the separator.*

Magnetic rigidity

Using equation 1.13 one can determine the magnetic rigidity of a nucleus traversing the FRS from its transversal x-positions at the second and fourth image planes:

$$B\rho = (B\rho)_c \cdot \left(1 + \frac{(x \mid x)_{24} x_4 - x_2}{(x \mid \delta p)_{24}}\right) \tag{1.15}$$

where $(x \mid \delta p)_{24}$ is the dispersion due to the first stage of the separator, x_2 and x_4 are the transversal positions at both image planes and $(B\rho)_c$ is the magnetic rigidity of the central-trajectory (section A.2). Two position-sensitive scintillators detectors [9] placed at the second and fourth image planes measure the transversal x-position (x_2 and x_4) in the range of ± 12 cm and ± 10 cm, respectively (see figure 1.4).

The resolution reached in $B\rho$ measurements can be calculated with the following equation:

$$\begin{aligned}\left(\frac{\Delta B\rho}{B\rho}\right)^2 &= \frac{1}{[(x \mid \delta p)_{24} + (x \mid x)_{24} x_4 - x_2]^2} \cdot \left[x_2^2 \left(\frac{\Delta x_2}{x_2}\right)^2 + (x \mid x)_{24}^2 x_4^2 \left(\frac{\Delta x_4}{x_4}\right)^2\right] \\ &+ \left(\frac{\Delta (B\rho)_c}{(B\rho)_c}\right)^2\end{aligned}$$

It should be noted that this resolution increases rapidly with increasing the dispersion. The $(B\rho)_c$ resolution is limited by the precision on the measurements of the magnetic rigidity for the central-trajectory $(B\rho)_c$. This resolution is normally about $\sim 10^{-4}$. In order to achieve a similar $B\rho$-resolution, the intrinsic resolution of the position detectors must be $\Delta x \sim 2$ mm for the typical range of x-positions.

Nuclear charge

The nuclear charge can be determined from energy-loss measurements (ΔE) performed with a MUlti-Sampling Ionisation Chamber (MUSIC) [10] placed at the exit of the separator (figure 1.4). Dependencies of the energy-loss on velocity must be corrected in order to obtain Z^2 from ΔE. Despite of these dependencies, the nuclear charge can be measured with high resolution, namely ΔZ=0.3 (FWHM).

Velocity

The velocity of the transmitted nuclei can be calculated from their time-of-flight. Scintillators SC2 and SC4 placed at the second and fourth image

planes, provide the start and the stop signal of the ToF; they have an intrinsic resolution of about 100 ps. The distance between both scintillators is 35 m. Corrections in the flight path due to the different trajectories of the nuclei inside the FRS must be included.

The mass resolution achievable with these measurements can be calculated from equation 1.14:

$$\frac{\Delta A}{A} = \sqrt{\left(\frac{\Delta B\rho}{B\rho}\right)^2 + \left(\frac{\Delta Z}{Z}\right)^2 + \frac{ToF^4c^4}{ToF^2c^2 - d^2} \cdot \frac{1}{d^2}\left(\frac{\Delta ToF}{ToF}\right)^2} \qquad (1.16)$$

This resolution is mainly limited by the resolutions in nuclear charge and time-of-flight, since they are, at least, one order of magnitude lower than that of the magnetic rigidity. By considering typical values of $ToF \simeq 150$ ns and $d \simeq 35$ m, it is possible to estimate a mass resolution value of $\sim 10^{-3}$. This result clearly demonstrates that the FRS in combination with the ToF and the MUSIC detectors is capable of identifying all ions up to the heaviest ones.

Unfortunately, the requirements on the mass resolution limit the acceptance of the FRS. Consequently, not all the fragments produced in the reaction will be transmitted through the FRS.

In the following chapter, we will discuss the problematic of the transmission of ions through an in-flight separator.

Chapter 2

Transmission of charged particles through in-flight separators

The transmission of charged particles through an in-flight separator depends on both, the kinematics of the reaction leading to the production of those particles and the maximum acceptance of the spectrometer. The acceptance is determined by the geometrical constraints and the ion-optical features of the apparatus.

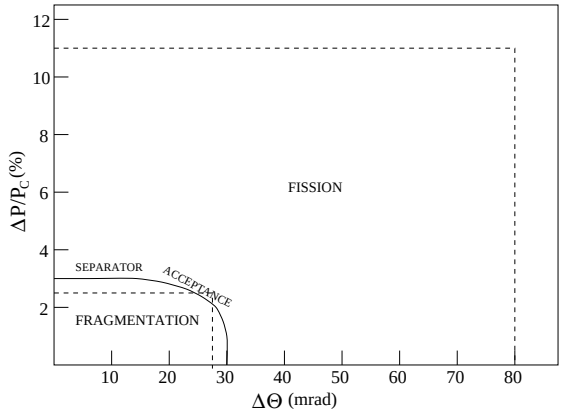

Figure 2.1: *Schematic representation of the angular and momentum spread for projectile residues produced in relativistic heavy-ion collisions. The solid line represents the limit of transmitted nuclei in standard in-flight separators.*

Figure 2.1 compares the angular and momentum acceptances of an in-

flight separator like the FRS with the typical angular width ($\Delta\theta$) and relative momentum spread ($\Delta p/p$) of nuclei produced in fragmentation and fission reactions. The area closed by the solid line represents those nuclei transmitted through the separator. The transmission of nuclei produced by fragmentation reaction is close to 100%, whereas for fission residues the transmission can be very low ($\leq 10\%$).

In this chapter we will explain in detail the two factors contributing to limit the transmission, namely, the acceptance of the spectrometer and the kinematics of the reaction.

2.1 Acceptances of in-flight separators

The transmission of the reaction residues through an in-flight separator is directly related to its acceptance. The geometrical constraints of the separator, as well as the ion-optical conditions defined by the magnetic elements limit this acceptance, which has typically maximum values of about ± 15 mrad and 3% in angle and relative momentum spread, respectively.

2.1.1 Longitudinal momentum acceptance

The momentum acceptance of the separator is determined by two factors:

- The geometrical transversal dimensions of the separator.
- The maximum dispersion of the dipole magnets.

As described in chapter 1, the transversal x-position of the transmitted nuclei and the maximum dispersion of the system at a dispersive image plane is connected with their magnetic rigidity through the equation 1.12. For a specific nucleus, these transversal positions are related to the momentum, since $B\rho \propto p$. In the case of the FRS, the maximum dispersion reached at the second image plane is -6.8 cm/%. The two quadrupoles placed directly before and after this image plane determine the maximum range in x-position, which is about $x_2 = \pm 10$ cm. Hence, the maximum momentum acceptance will be:

$$\left(\frac{\Delta p}{p_c}\right)_{max} = \frac{x_2}{(x \mid \delta p)_{02}} \simeq \pm 1.5\% \tag{2.1}$$

This equation clearly shows that the momentum acceptance can be increased by reducing the dispersion. However, as already mentioned in section 1.2, a lower dispersion at the second image plane reduces the $B\rho$-resolution necessary to identify the heaviest masses. Therefore, the dispersion value given

by the dipole magnets is a compromise between the momentum acceptance and the $B\rho$-resolution.

2.1.2 Angular acceptance

The reaction residues enter into the separator with an angular distribution determined by the reaction mechanism. Nuclei with angles higher than the angular acceptance of the separator will not be transmitted.

The angular acceptance of an in-flight separator depends on the transversal dimensions of the system and its ion-optical characteristics. The transversal size of the separator is mainly determined by the gap of the magnetic elements, (dipoles and quadrupoles). In principle, one could increases these gaps in order to enhance the angular acceptance. On the other hand, this implies a variation of the ion-optical conditions in such a way that the magnetic fields should be increased to set the previous conditions. Therefore, the maximum achievable magnetic field ($\sim$ 1.6 T) leads to a maximum value of these gaps.

In order to calculate the angular acceptance, one should find an equation similar to 2.1 relating the transversal x-position of the transmitted nuclei with their angle and with the ion-optical characteristics of the separator. This is not possible in this case, since the relation between the angles and the x-position is very complicated. Therefore, the angular acceptance must be determined either from experimental results or by numerical calculations. This problematic will be explained in chapter 4 where we describe a new method developed to calculate the angular acceptance with very high precision.

2.2 General overview on Kinematics

In the study of the transmission, it is important to know in detail the kinematics of the reactions products. Collisions between heavy ions at relativistic energies lead to excited nuclei which deexcitate by evaporating particles or by fissioning. The final angular and momentum distributions of the reaction products will be determined by the different kinematics of both reaction mechanisms.

2.2.1 Fragmentation reactions

The kinematic of nuclei produced in projectile-fragmentation reactions is mainly determined by two effects: the Fermi momentum of the nucleons

abraded in the interaction between the projectile and the target, and the later evaporation of nucleons from the excited projectile residue.

In the frame of the Fermi-gas model, the momenta of the nucleons follow a Gaussian distribution. The sum of these momenta is zero in the centre-of-mass frame of the nucleus:

$$\vec{P}_{CM} = \sum_{i=1}^{N} \vec{p}_i = 0 \tag{2.2}$$

where $\vec{P}_{CM}$ is the momentum of the nucleus in the centre-of-mass frame, N is the number of nucleons and $\vec{p}_i$ is the momentum of each nucleon. After the collision, some nucleons from the projectile will be ejected, while the projectile-like residue (prefragment) will gain some excitation energy. Due to the momentum conservation, the ejected nucleons and the prefragment will have opposite momenta in the centre-of-mass frame:

$$\vec{P}^{f}_{CM} = \sum_{i=1}^{N-n} \vec{p}_i = -\sum_{i=1}^{n} \vec{p}_i \tag{2.3}$$

where $\vec{P}^{f}_{CM}$ is the momentum of the prefragment in the centre-of-mass frame and n is the number of ejected nucleons. Since the momenta of the ejected nucleons are taken from a Gaussian distribution, it can be concluded that the same kind of distribution is found for the momentum of the prefragments.

Taking these considerations into account, Goldhaber calculated the width of this Gaussian distribution for the longitudinal momentum component [11]:

$$\sigma(p_{\|}) = \frac{p_F}{\sqrt{5}} \sqrt{\frac{A_f(A_p - A_f)}{A_p - 1}} \tag{2.4}$$

where p_F is the Fermi momentum of the nucleons, A_p is the mass of the projectile and A_f is the mass of the fragment.

Later, Morrisey determined a semiempirical parametrisation of $\sigma(p_{\|})$, including the effect of the evaporation of nucleons from the excited projectile residue, which leads to a broadening of the longitudinal momentum distribution [12]:

$$\sigma(p_{\|}) = \frac{150}{\sqrt{3}} \sqrt{A_p - A_f} \tag{2.5}$$

It has also been experimentally determined that $\sigma(p_{\|})$ is equal to $\sigma(p_{\perp})$ to within 10%. Therefore, to calculate the width of the angular distribution in the beam frame -roughly the laboratory frame-, one has to divide $\sigma(p_{\perp})$, calculated with equation 2.4 or 2.5, by the longitudinal momentum

component. In the laboratory frame, the distribution of the longitudinal component is approximately centred at the momentum of the beam. On the other hand, since $\sigma(p_{\parallel})$ is much lower than this value, to estimate the angle one can assume that the prefragment is always produced with a longitudinal momentum equal to that of the beam. Therefore, the value of $\sigma(\theta)$ for the studied nucleus will be:

$$\sigma(\theta) \simeq \frac{\sigma(p_{\perp})}{p_{beam}} \tag{2.6}$$

From equations 2.4 or 2.5 and 2.6, we can estimate the angular and the momentum distribution for a typical nucleus produced in the projectile-fragmentation of ^{208}Pb(500 A MeV), like ^{179}Hf. The width of the distribution calculated with the Morrisey equation is $\sigma(p_{\parallel}) = 468.5$ MeV/c, which means a relative momentum spread of $\sim \pm 0.1\%$. The width of the angular distribution is: $\sigma(\theta) = \frac{\sigma(p_{\parallel})}{p_{beam}} \simeq 2$ mrad with $p_{beam} = 22.6 \times 10^4$ MeV/c. Since the acceptance values of the separator are about 3%, for the relative momentum spread and and ± 15 mrad for angular spread, one concludes that the transmission in this case is close to 100%. For fragments much lighter than the beam, the transmission can be reduced down to $\sim 80\%$.

2.2.2 Fission reactions

The kinematics of fission reactions is determined by the Coulomb repulsion between both fission fragments. The kinetic energy of these residues can be calculated with the following equation

$$TKE = \frac{Z_1 \cdot Z_2 \cdot e^2}{D} \tag{2.7}$$

where Z_1 and Z_2 are the nuclear-charge of the two fission products and D is the distance between the centre of both fragments at the scission point, which can be calculated from the Wilkins model [13]:

$$D = r_0 A_1^{1/3} \left(1 + \frac{2}{3}\beta_1\right) + r_0 A_2^{1/3} \left(1 + \frac{2}{3}\beta_2\right) + d \tag{2.8}$$

where $r_0 = 1.16$ fm, A_1 and A_2 are the masses of the fragments, $d \simeq 2$ fm and β_1, β_2 are the coefficients of deformation.

The final momentum distribution of the fission residues is spherical in the centre-of-mass frame of the reaction with a radius given by the kinetic energy calculated with the equation 2.7. Due to the Lorentz transformation from the centre-of-mass frame into the laboratory frame, this spherical distribution becomes an ellipsoid.

In the case of a typical fission product like ^{104}Nb with a kinetic energy of $\sim$ 800 A MeV in the laboratory frame, the angular and momentum spread are about $\pm$30 mrad and 10%, respectively. If these values are compared with the acceptances of the FRS, one realises that the transmission of such products is quite low. As already mentioned in the introduction of this chapter, typical values of this transmission are lower than 10%.

Figures 2.2 and 2.3 illustrate the effect of the limited momentum and angular acceptance for the fission residues. These nuclei populate the border of the ellipsoid in the momentum space. The centre of this ellipsoid roughly corresponds to the beam momentum. Figure 2.2 schematically represents the cuts in the momentum distribution of fission residues due to the limited momentum acceptance.

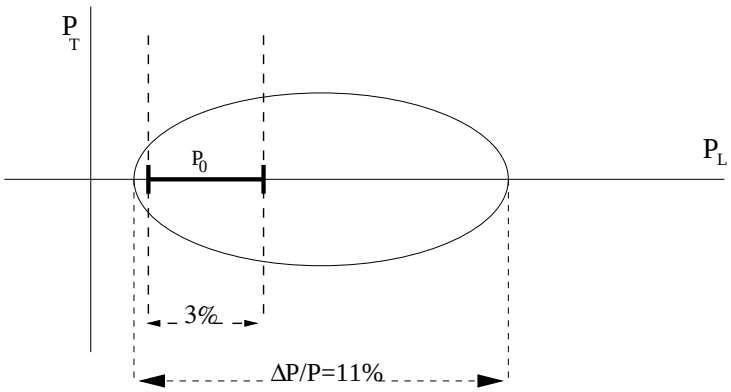

Figure 2.2: *Schematic representation of the momentum distribution in the laboratory frame of fission residues produced in heavy-ion collisions. P_T and P_L represent the transversal and longitudinal momentum, respectively. The solid segment represents the typical momentum acceptance of an in-flight separator, and P_0 is the momentum of the particle following a trajectory centred along the optical axis of the FRS. Only nuclei with momentum deviations of $\pm$1.5% (3%) will be transmitted through the spectrometer.*

Those nuclei with momentum p_0 follow a trajectory centred along the optical axis of the FRS. The figure shows that only nuclei with momentum deviations of $\pm$1.5% can pass through the spectrometer. This problem can be solved by sweeping the whole range of momentum in different settings (changing the magnetic fields of the dipoles), so that the full distribution of fragments can be reconstructed by superposing all the settings. In this way, the full momentum distribution can be measured in spite of the limited momentum acceptance of the spectrometer.

In figure 2.3, we depict the cuts in the momentum distribution of the

fission residues due to the limited angular acceptance of the separator. In the space of momenta, the angular acceptance defines a cone which cuts the ellipsoidal distribution. Only those nuclei inside the cone will be transmitted.

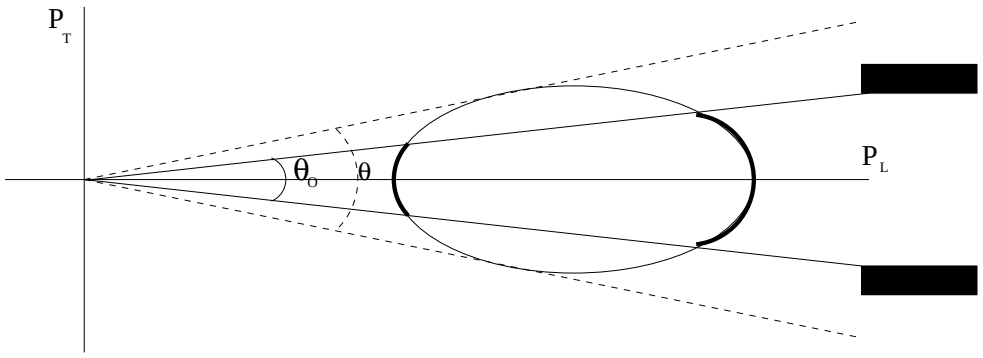

Figure 2.3: *Angular acceptance of the FRS cutting the ellipsoidal distribution of fission fragments ($\theta \simeq \pm 30$ mrad) in the space of momenta. Only nuclei with angles lower than θ_0 mrad will be transmitted through the spectrometer.*

Chapter 3

Experimental results

The angular and momentum distribution of fission residues produced in relativistic heavy-ion collisions are larger than the acceptance of most of the standard in-flight separators. Therefore, only part of the reaction residues will be transmitted through the spectrometer. The transmission cuts produced by the spectrometer can be studied experimentally by comparing the full angular and momentum distributions measured just after the fission reaction takes place with those obtained with the spectrometer.

In this chapter, we will present the analysis of two different experiments:

In the first experiment, a large-acceptance energy-loss, ToF set-up was used to measure the full angular and velocity distribution of fission residues produced in the reaction ^{238}U(1 A.GeV)+p. This set-up does not provide a full isotopic identification of the reaction residues.

The second experiment was intended to identify fission residues produced in the same reaction as the previous one, but using the FRS with its standard detection equipment. In this case we are able to identify the isotopes produced in the reaction but the angular and velocity distribution of these residues is cut by the limited acceptance of the FRS.

A comparison of the momentum (or velocity) distribution of the fission fragments obtained in both experiments will show, how the angular acceptance of the separator dramatically reduces the transmission of fission residues.

3.1 Angular and velocity distribution of fission residues

In the first experiment, the full angular and velocity distribution of fission fragments were measured. The uranium primary beam at 1 A GeV passes

through the FRS and hits the plastic target placed at the fourth image plane producing the fission residues. The set-up at the end of the separator is schematically represented in figure 3.1.

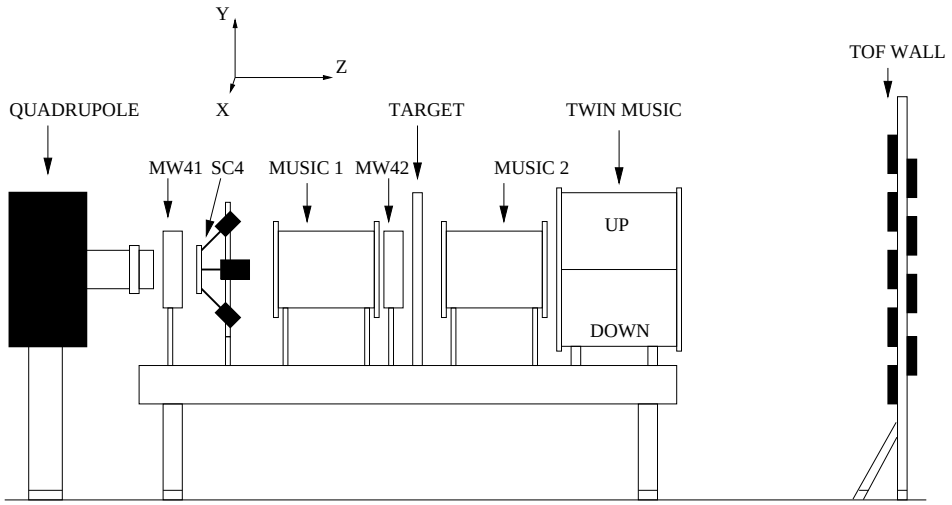

Figure 3.1: *Experimental set-up used to measure the full velocity and angular distribution of the fission fragments.*

Figure 3.2 illustrates how the two MUSICs [10] behind and in front of the target are used to determine where the fission residues are produced: since the signal collected in the ionisation chambers is proportional to the charge squared, the beam passing through the MUSIC 1 generates the highest signal, whereas the reaction products generate a lower signal in MUSIC 2 (window C and E) . If no reaction takes place and the beam passes through the two MUSICs, two high identical signals are collected in both detectors (window A). If the reaction is not produced in the target but in the scintillator SC4, the two ionisation chambers give the same signals, lower than those produced by the projectiles (windows B and D).

The two multiwires detectors MW41 and MW42 are used to check whether the primary beam hits the target at the central position.

The TWIN-MUSIC [14] is a segmented ionisation chamber. Its design allows the measurement of the transversal x and y coordinates of the detected nuclei. Finally, the scintillators wall [14], together with the scintillator SC4 are used to determine the velocity of the fission residues from the time-of-flight measurements, and to calibrate the vertical y positions of these nuclei in the TWIN-MUSIC.

In next section, we will explain how the angles and the velocities of the produced nuclei are determined.

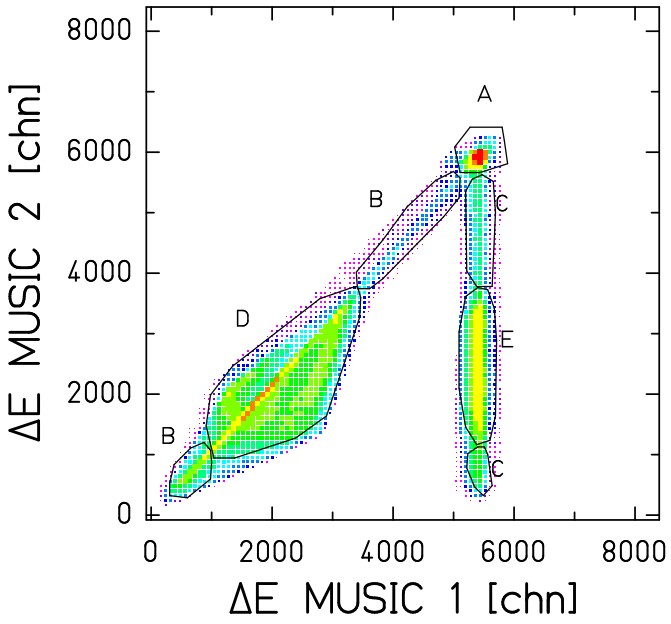

Figure 3.2: *Cluster plot of the signal intensities of the MUSIC 1 and MUSIC 2. Fission residues from the scintillator SC4 and from the target correspond to windows D and E, respectively. Windows B and C represent the fragmentation products from SC4 and from the target. The signal produced by projectiles passing through both MUSICs corresponds to window A.*

3.1.1 Determination of angles

The transversal angles (θ and ϕ) of the fission residues correspond to the planes x-z and y-z, respectively (see figure A.5). These angles are determined by means of the TWIN-MUSIC:

This detector is divided in two ionisation chambers, one above the other, which are separated by a common cathode. Eight anodes are placed on the top of the upper TWIN-MUSIC and on the bottom of the lower TWIN-MUSIC (see figure 3.3). The special geometry of the anodes allows the measurement of the x coordinates (see figure 3.3). The y coordinate is given by the drift time:

When the fission reaction takes place, each fission fragment is detected in one of the ionisation chambers of the TWIN-MUSIC. Their transversal x

coordinate can be calculated as:

$$x(mm) = 300 \cdot \frac{Q^l - Q^r}{Q^l + Q^r} \tag{3.1}$$

where x is the transversal coordinate, Q^l and Q^r are the electric charges collected by the anodes placed on the left and right sides of the TWIN-MUSIC. The factor 300 corresponds to the thickness of the TWIN-MUSIC (300 mm).

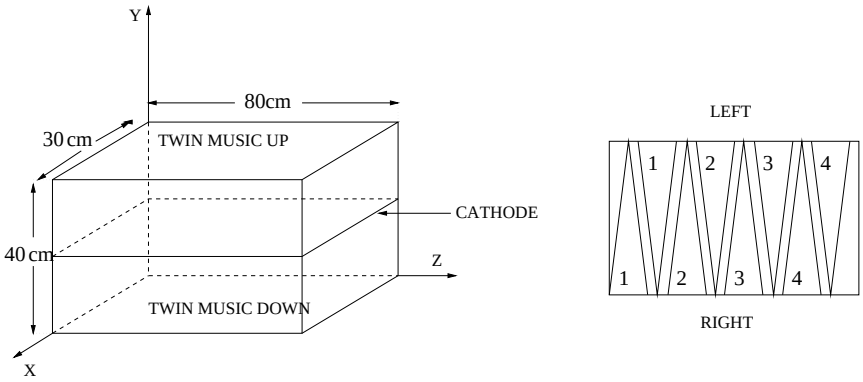

Figure 3.3: *The TWIN-MUSIC is a two segmented ionisation chamber. The cathode is placed in the middle, whereas the anodes are on the top and bottom of the detector. Right: top view showing the shape of the anodes.*

The vertical coordinates (y) of the fission residues are determined by measuring the drift time, in such a way that y will be expressed as a function of this time according to the following equation:

$$y = aT_{drift} + b \tag{3.2}$$

where T_{drift} is the measured drift time and a and b are coefficients which must be determined from the y-position calibration of the TWIN-MUSIC. This calibration was done with the scintillator wall (ToF-Wall):

The ToF-wall consists of 16 paddles of scintillators with two photomultipliers placed at both extremes of each paddle (see figure 3.4).

The vertical coordinate of the paddle (y coordinate) hit by each fission fragment is known. Then, the y coordinates of the nuclei in the TWIN-MUSIC are given by (see figure 3.5):

$$y_{up} = d \cdot \frac{y_{up}^{pad}}{L} \tag{3.3}$$

$$y_{down} = d \cdot \frac{y_{down}^{pad}}{L} \tag{3.4}$$

where d is the distance from the target to the TWIN-MUSIC (2.457 m), L is the distance from the target to the scintillators wall (5.456 m) and y_{pad}^{up} and y_{pad}^{down} are the vertical coordinates of the paddles hit by the fission fragments.

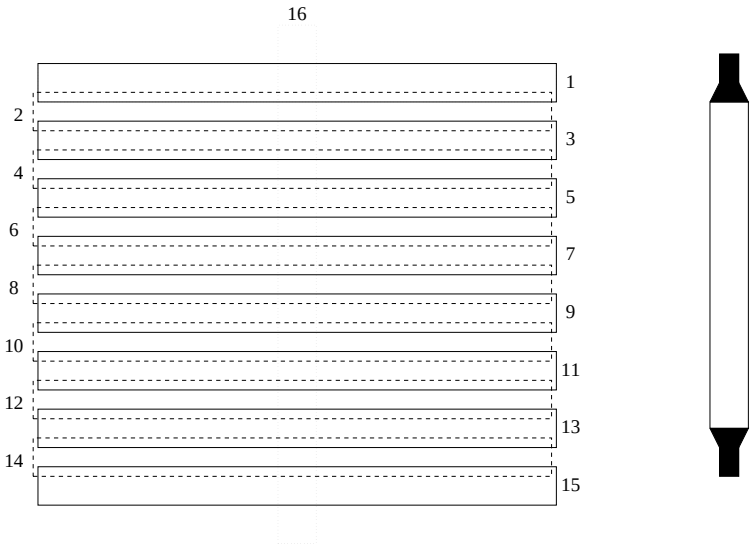

Figure 3.4: *The ToF-wall made of 16 scintillator paddles. Right: view of one paddle with a photomultiplier at each extreme.*

The position calibration of the TWIN-MUSIC is done by comparing the drift time signals with the vertical coordinate calculated with equations 3.3 and 3.4. From this calibration we obtain the coefficients a and b of equation 3.2, so that the vertical coordinates of the fission residues traversing the TWIN-MUSIC will be calculated from T_{drift} with this equation.

Finally, the transversal angles can be obtained from the expressions:

$$\theta_{up} \simeq \tan(\theta_{up}) = \frac{x_{up}}{d} \tag{3.5}$$

$$\theta_{down} \simeq \tan(\theta_{down}) = \frac{x_{down}}{d} \tag{3.6}$$

$$\phi_{up} \simeq \tan(\phi_{up}) = \frac{y_{up}}{d} \tag{3.7}$$

$$\phi_{down} \simeq \tan(\phi_{down}) = \frac{y_{down}}{d} \tag{3.8}$$

where θ and ϕ are the transversal angles in the horizontal and vertical directions, respectively. The indexes *up* and *down* refer to the coordinates

measured by the upper and lower TWIN-MUSIC. d is the distance between the target and the TWIN.

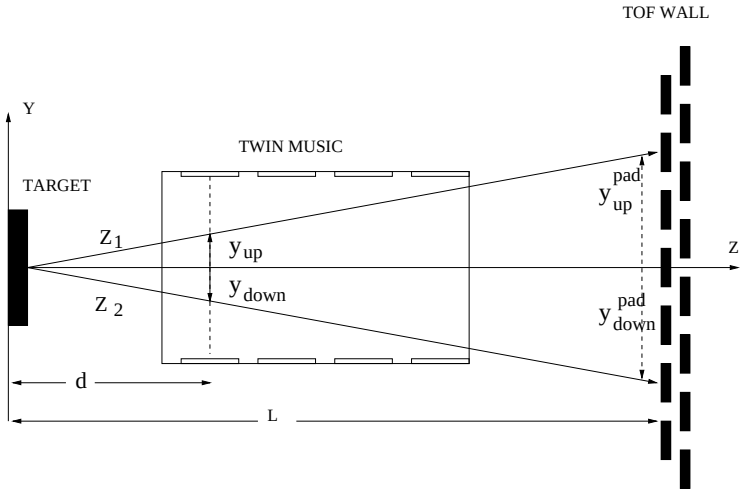

Figure 3.5: *The vertical coordinate y_{up} and y_{down} of the two fission fragment (Z_1 and Z_2) in the TWIN-MUSIC are calculated from the y coordinates of the hit paddles.*

3.1.2 Determination of the velocity

The velocities of the fission residues are obtained from the time-of-flight measurement (ToF) between the passage of the beam through the start detector SC4, and the arrival of both fission fragments to the ToF-Wall. From this measured ToF, the time-of-flight of the beam (ToF_{beam}) from SC4 to the middle of the target, was substracted in order to obtain the time-of-flight of the two fission fragments ($ToF_{fission}$). The time-of-flight of the beam was theoretically calculated as the integral $ToF_{beam} = \int 1/v_{beam}(z)dz$ where $v_{beam}(z)$ is the velocity of the beam calculated step by step including the energy loss in the layers of matter along the flight path.

An unknown offset parameter in the time-of-flight calibration for the time-of-flight from SC4 to the ToF-Wall was calibrated by comparing the measured ToF with the integral $\int 1/v(z)dz$ in order to take into account the energy loss of the beam and fission residues through the different layers of matter. In this integral, $v(z)$ is the velocity along the flight-path z. Since the energy loss of the nuclei depends on their charge, we considered an average charge for the fission residues equal to half of the value of the beam (92/2).

The velocity of the fission nuclei ($v_{fission}$) can be determined by dividing the calculated $ToF_{fission}$ by the flight path of these nuclei. The angular range populated by the fission fragments is so small that their flight paths coincide with the distance from the target to the scintillators wall (L=5.5 m) within 0.1%, so that the velocity is calculated with equation:

$$v_{fission} = \frac{L}{ToF_{fission}} \tag{3.9}$$

3.2 Angular and velocity distribution of fission fragment with the FRS

In the second experiment, the target was placed at the entrance of the FRS. A uranium beam at 1 A GeV hits an hydrogen target producing the fission residues. These nuclei were identified by using the FRS as has been described in chapter 1.

Figure 3.6 shows the detectors used in this experiment. The time-of-flight of the transmitted nuclei was measured between the plastic scintillators SC2 and SC4. Multiwires detectors MW41 and MW42 were used to measure the angles of the nuclei while the MUSICs ionisation chamber provided the charge identification.

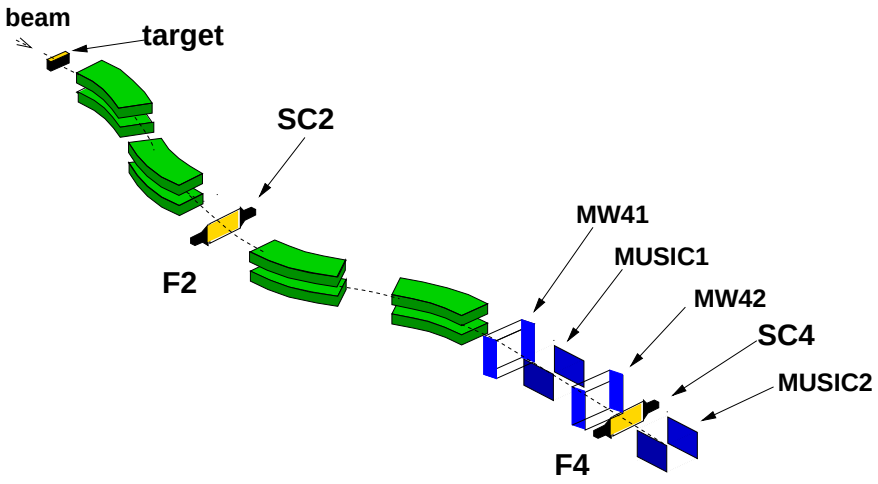

Figure 3.6: *Experimental Set-up used to identify reaction residues with the FRS. Scintillators and multiwire detectors were used to measure the time-of-flight and the angles of the nuclei, respectively. The charge identification was done with the MUSICs.*

For the purpose of this work it is not worthwhile to enter into the details of the identification procedure, which has already been explained in chapter 1. Therefore, we will rather restrict ourselves to the part of the analysis related to the determination of the angular and velocity distribution. As in the previous experiment, we want to determine the angular distribution of the fission fragments and the correlation between the horizontal transversal angle and the velocity.

3.2.1 Determination of angles

The nuclei produced in the target by fission reactions enter into the separator with different angles. In order to determine the angular distribution of the transmitted nuclei, we must measure the angles of these nuclei at the entrance of the FRS. Unfortunately, this can not be carried out because there was no position-sensitive detectors mounted between the target and the entrance of the spectrometer. The angles of the transmitted nuclei are modified by the magnetic elements placed along the FRS. These angles at the fourth image plane can be expressed as a function of the coordinates of the fission fragments at the entrance of the FRS (appendix A):

$$\begin{aligned} \theta_4 &= (\theta \mid x)_{04} x_0 + (\theta \mid \theta)_{04} \theta_0 + (\theta \mid y)_{04} y_0 + (\theta \mid \phi)_{04} \phi_0 + (\theta \mid \delta p)_{04} \delta p_0 \\ \phi_4 &= (\phi \mid x)_{04} x_0 + (\phi \mid \theta)_{04} \theta_0 + (\phi \mid y)_{04} y_0 + (\phi \mid \phi)_{04} \phi_0 + (\phi \mid \delta p)_{04} \delta p_0 \end{aligned}$$

where we only include first order terms. x, y, θ and ϕ are the coordinates of the nuclei (see figure A.5) and δp is the relative momentum spread. The subscripts 0 and 4 stand for the coordinates at the target and at the fourth image plane. Due to the magnetic characteristics of the FRS, only $(\theta \mid \theta)_{04}$ and $(\phi \mid \phi)_{04}$ (the so-called angular magnifications) are not negligible. Since the values of these angular magnifications are known, the angular distribution just behind the target can be deduced from that measured at the fourth image plane:

$$\theta_0 = \frac{\theta_4}{(\theta \mid \theta)_{04}} \tag{3.10}$$

$$\phi_0 = \frac{\phi_4}{(\phi \mid \phi)_{04}} \tag{3.11}$$

The measurement of the angles is performed by two multiwire chambers (MW41 and MW42) placed at the end of the FRS (see figure 3.6). These detectors are sensitive to both x and y transversal coordinates. The angles

at the fourth image plane can be calculated with the following equations:

$$\theta_4 \simeq \tan\theta_4 = \frac{x(MW42) - x(MW41)}{d} \tag{3.12}$$

$$\phi_4 \simeq \tan\phi_4 = \frac{y(MW42) - y(MW41)}{d} \tag{3.13}$$

where $x(MW41)$ and $y(MW41)$ are the transversal positions measured by the multiwire MW41, $x(MW42)$ and $y(MW42)$ are the same variables measured by the multiwire MW42, and d is the distance between both detectors (1.071 m).

3.2.2 Determination of the velocity

The time-of-flight of the nuclei transmitted through the separator is measured with two plastic scintillators [9] placed at the second and fourth image planes (SC2 and SC4):

$$ToF = T_4 - T_2 \tag{3.14}$$

where $T_4 - T_2$ is the time difference measured between the scintillators SC4 and SC2. Both detectors were read out by two photomultipliers placed on the left and right, so that T_4 and T_2 are the medium values between the times measured by each photomultiplier:

$$T_4 = \frac{T_4^l + T_4^r}{2}$$

$$T_2 = \frac{T_2^l + T_2^r}{2}$$

where the indexes l and r stand for the times measured by the photomultipliers on the left and right, respectively.

The start signal of the ToF measurement is produced when the nucleus reaches the scintillator SC4. The stop signal is generated by the signal coming from the scintillator SC2 plus a delay T_0. Therefore, what we measure experimentally is not the real time-of-flight described in equation 3.14 but:

$$\begin{aligned} ToF^* &= (T_2 - T_4) + T_0 \\ &= -ToF + T_0 \end{aligned} \tag{3.15}$$

T_0 must be deduced from the ToF calibration, which was done by comparing the measured ToF^* with the velocity v deduced from the magnetic rigidity of the primary beam when it traverses the whole separator. These two quantities are related to each other through the following equation:

$$ToF^* = -\frac{L}{v} + T_0 \tag{3.16}$$

where L is the path traversed by the beam between SC2 and SC4 and v is its velocity. If one represents the measured ToF^* at different velocities of the beam as a function of $1/v$, the quantities L and T_0 can be deduced by a linear fit. Once T_0 was calculated, the real time-of-flight (ToF) of the transmitted nuclei can be easily deduced from the measured ToF^*. Finally, the velocity of these fragments is calculated by dividing the distance between SC2 and SC4 (35 m) by the time-of-flight. However, the trajectory followed by the nuclei is not a straight line and hence, this distance must be corrected by including an angular dependence.

3.3 Results

The angular and the velocity distribution of a nucleus produced in fission reactions before and after being transmitted through the FRS must be compared in order to see how the separator affects the transmission of this fission fragment. This could be done in the two experiments described above. Nevertheless, the masses of the fission residues can not be determined in the first described experiment, so that these nuclei were not identified. For that reason, our analysis shows the angular and velocity distribution of several nuclei produced in fission reactions without taking into account neither their masses nor their charges. Figure 3.7 depicts the results of this analysis. The upper part of figure 3.7 compares the velocity distributions of the fission fragments obtained in both experiments. The horizontal axis represents the longitudinal velocity, whereas the angle θ corresponds to the vertical axis. In the left figure, the ellipsoidal velocity distribution of the fission fragments is reconstructed. The right figure represents the velocity distribution of the nuclei transmitted through the separator. As can be seen, only nuclei emitted on forward and backward direction reach the fourth image plane. The centre-of-mass velocity, which is roughly equal to that of the beam, is 1 cm/ns faster for the experiment with the target placed at the entrance of the FRS. This is due to the fact that the beam had to cross several layers of matter (SC41, MUSIC 1 ,MW42) before arriving to the target, in the first experiment.

The lower part of figure 3.7 shows the whole angular spread of fission residues compared with that measured with the FRS: In the left figure, the reaction products have angles distributed in a range of approximately ± 40 mrad. One of the requirements to accept a fission event is that two different paddles of the TOF-WALL give a signal produced for each fission residue in coincidence. However, the two fission residues can be produced with a vertical angle ϕ equal to zero so that only the central paddle is hit by both fragments. In addition, those events where both fission fragments hit

the same part of the TWIN-MUSIC are disregarded. This explains the lack of counts for $\phi = 0$ in the picture. The right figure represents the angles of the nuclei transmitted through the separator. From this figure, one estimates an angular acceptance value of about ± 15 mrad.

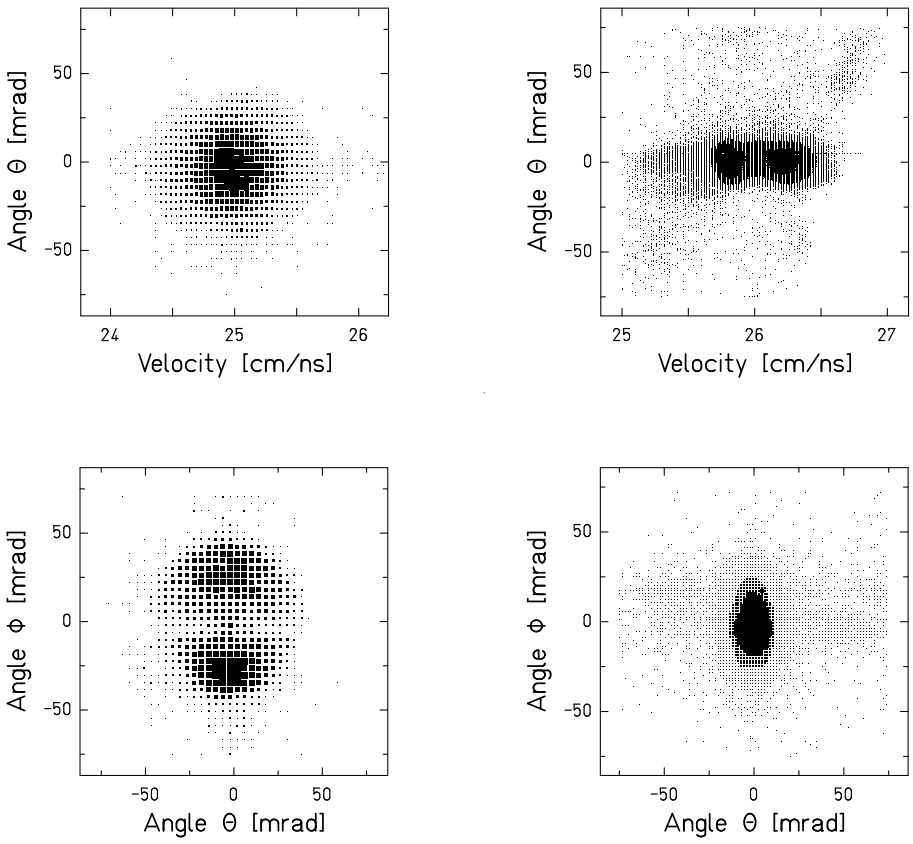

Figure 3.7: *Upper part. Left: full velocity distribution of nuclei produced in fission reactions. Right: the same distribution after passing through the separator, only nuclei emitted on forward and backward direction are transmitted. Lower part. Left: full transversal angular distribution of nuclei produced in fission reactions. Right: the same distribution for the nuclei transmitted through the FRS.*

3.4 Angular transmission evaluation

From the experimental results described above, one could calculate the angular transmission of fission residues through the FRS. In the first experiment, the total number of nuclei produced in the fission reaction can be detected, whereas in the second experiment only those fission residues reaching the fourth image plane of the FRS are measured. Therefore, the transmission will be the ratio of nuclei measured in the second experiment to those measured in the first one. The detection efficiency for the experiment measuring the total number of fission nuclei must be as large as possible in order to obtain a precise value of this transmission. The detectors used to measure the total number of fission residues were the TWIN-MUSIC and the TOF-WALL. The condition required to accept a fission event is that the two ionisation chambers of the TWIN-MUSIC and two different paddles of the TOF-WALL give a signal in coincidence. Nevertheless, it is possible that the two fission residues traverse only one part of the TWIN-MUSIC. This is due to the angular spread of the beam, which leads to a change in the direction of flight of the produced nuclei. In addition, the nuclei produced with an angle ϕ equal to zero hit only the central paddles. The detection efficiency was calculated with a simulation code including the mentioned conditions to accept a fission event. The calculation gives an efficiency of $\sim 80\%$, which is sufficiently high to measure the angular transmission with the required precision. Nevertheless, such a measurement represents a great effort which we would like to avoid if possible. In addition, the measurement of the total number of fission fragments in the first experiment does not provide a full isotopical identification and therefore, one cannot determine the transmission for specific nuclei.

However, one can roughly estimate the angular transmission from the pictures shown in figure 3.7. The transmission is the ratio of the fission residues transmitted through the FRS to the total number of nuclei produced in the reaction. This ratio is roughly equal to that obtained between the surfaces of the region populated by the transmitted nuclei (right picture in the upper part of figure 3.7) and the surface of the total ellipsoidal distribution in the space of velocities (left picture in upper part of figure 3.7). Both surfaces can be estimated from figure 3.7. The velocity corresponding to the centre of the ellipsoidal velocity distribution is $v_0 = 25.0$ cm/ns and the maximum angle of the fission residues is about ± 40 mrad, so that the maximum transversal velocity of these nuclei is 1 cm/ns. This defines one of the axis of the ellipsoid (a). The other axis (b) is the difference between v_0 and the maximum or the minimum longitudinal velocities of the fission residues. This difference is about 0.6 cm/ns. Therefore the surface of the ellipsoid is equal to

$S_{ellipsoid} = \pi ab = 2$ cm^2/ns^2. The right picture in the lower part of the same figure shows the forward and backward regions of the ellipsoid transmitted through the FRS. As explained above, the velocities of the transmitted nuclei shown in this picture are 1 cm/ns higher than those of the nuclei produced in the target at the fourth image plane. Therefore, one must correct for this difference in order to compare the surfaces populated by the transmitted nuclei with $S_{ellipsoid}$. The transmitted regions of the ellipsoid have roughly a circular shape. Their surface is equal to $\pi v_\perp^2$ where $v_\perp$ is the transversal velocity of the transmitted fragments. The maximum angle of these nuclei is about ± 15 mrad and their longitudinal velocity is 24.4 cm/ns, for the backward emitted fragments and 25.6 cm/ns, for those emitted on forward direction. Therefore, the traverse velocities are 0.36 cm/ns and 0.38 cm/ns. From these velocities, we can calculate the surfaces populated by the backward and forward emitted fragments, which are $S_{backward} = 0.40$ cm^2/ns^2 and $S_{forward} = 0.43$ cm^2/ns^2 respectively. Finally, the transmission that we estimate for the the backward and forward emitted fission residues is:

$$T_{backward} = \frac{S_{backward}}{S_{ellipsoid}} = 20\%$$
$$T_{forward} = \frac{S_{forward}}{S_{ellipsoid}} = 21\%$$

The calculations shown above are a very rough estimation of the angular transmission. It clearly demonstrates that the losses are very important but it is not intended to give precise results. A more detailed determination of the transmission must be done for each isotope, since the kinematics depends on the nucleus studied, as explained in chapter 2. The full analysis of the experimental data considered in the present chapter including the isotopic identification of the reaction products is beyond the scope of the present work.

3.5 Conclusions

The analysis of the experimental data of two experiments has shown that the limited angular acceptance of the FRS allows only two distinct parts of the velocity distribution of the fission fragments to pass through: those emitted either in forward or in backward direction. This leads to a typical double-humped velocity distribution. The angular transmission is rather small, in the order of 10%. Experiments to measure the angular transmission need additional beam time. They are actually not able to determine the angular

transmission for specific isotopes. This emphasises the need for reliable and precise model calculations.

Chapter 4

Angular transmission evaluation

The transmission of nuclei through an in-flight separator like the FRS depends on two factors: the kinematics of the reactions producing the residues and the acceptances of the separator. Monte-Carlo codes like MOCADI [15] calculate this transmission by simulating the transport of the nuclei through the separator. In these codes, the trajectories of the ions depend on the kinematics of the reaction, and the magnetic characteristics of the separator. In addition, the geometrical constraints are taken into account in order to check whether the nuclei are transmitted or not.

Until now, the transmission was calculated for each nucleus separately, since the kinematics depends on their mass and charge. The time needed to perform one Monte-Carlo simulation is about 10 minutes. Therefore, for experiments where more than 1000 nuclei are produced, we can not afford for such calculation times.

In the present work, we describe a new method which minimises the time necessary to determine the transmission of any nuclei through the FRS. The main idea of this method is to determine a map of the angular acceptance of the separator as a function of global variables characterising the trajectory of any particle. The method was developed in two steps:

Firstly, the angular acceptance of the FRS is calculated with a Monte-Carlo code which simulates the transport of nuclei through the separator. This acceptance depends on the trajectories followed by the nuclei along the FRS, which will be parametrised by global variables. As will be seen later, these global variables are the transversal x-position at the second and fourth image planes, so that this procedure will provide a map of the angular acceptance as a function of x_2 and x_4.

Secondly, the transmission of any nucleus will be analytically determined

by considering both, the angular acceptance $\alpha(x_2, x_4)$, corresponding to its trajectory defined by the x-position at the second and fourth image planes (x_2, x_4) and the kinematics due to the reaction mechanism.

In the first part of the chapter, we will explain the design of the Monte-Carlo code which we have developed to reconstruct the acceptance map of the separator. In the second part, we will describe in detail how the final transmission values are determined taking into account the acceptance map and the kinematics of the reaction.

4.1 Transport code for ion-optic calculations

In order to get accurate values of the angular acceptance, the transport of nuclei through the separator must be simulated with high precision. Two factors enter into this simulation: the trajectories followed by the nuclei inside the FRS and the geometrical constraints of the separator.

4.1.1 Simulation of the trajectories

The trajectory of a nucleus in a magnetic system is described by a set of coordinates (see appendix A): the transverse positions x and y, the longitudinal position s, the transverse angles θ and ϕ, and the relative deviation from the reference momentum δp. The evolution of these coordinates along the separator depends on their initial values and the magnetic properties of the system.

The FRS consists of several magnetic elements which determine the trajectories of the nuclei. The magnetic characteristics of each magnet are simulated by means of a matrix formalism (see appendix A). Many ion-optical codes, such as GICO [16], can be applied to calculate the transfer matrices of any magnetic system. The matrices, obtained from these calculations including third order terms were used by our code. The trajectories of the nuclei through the FRS are reconstructed by multiplying the vectors describing the nuclei at the entrance of the FRS by all these matrices.

4.1.2 Geometrical constraints

The region traversed by the nuclei through the FRS is limited by the dimensions of the tubes placed inside the magnetic elements. The transmission of the nuclei through the separator depends on both the transverse dimensions and the shape of these tubes. Figure 4.1 represents these two factors for the different magnetic elements placed along the FRS.

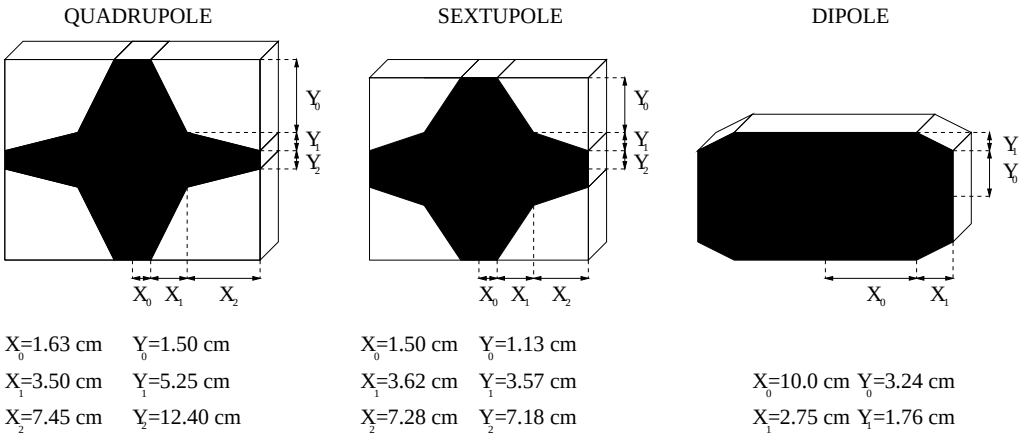

Figure 4.1: *Shape and dimensions of the inner tubes inside the different magnetic elements of the FRS. Left: quadrupoles. Centre: sextupoles. Right: dipoles.*

In order the check whether the nuclei are transmitted through the separator or intercepted by the walls of the tubes, the program compares the transverse coordinates (x and y) of the nuclei with the dimensions of the tubes. This is done behind, in the middle and in front of each magnetic element.

Detector	Dimension x (cm)	Dimension y (cm)	Experimental Area
Scintillator SC2	± 11	± 4	Second image plane
Scintillator SC4	± 10	± 4	Fourth image plane
Multiwire MW41	± 10	± 10	Fourth image plane
Multiwire MW41	± 10	± 10	Fourth image plane

Table 4.1: *Transversal dimension of detectors at the second and fourth image planes.*

In addition, several detectors are placed along the FRS with transverse dimensions different of those shown in figure 4.1. These dimensions are included into the simulations, since they affect the transmission of nuclei. Table 4.1 shows the transverse dimensions of the different standard detectors

used with the FRS. The angular straggling due to these detectors was also included in our calculations.

4.2 Angular acceptance of the FRS

In order to check whether a nucleus is transmitted through the FRS, we have to compare its transversal coordinates x and y at any longitudinal position with the dimensions of the tube placed inside the magnetic elements. These coordinates are functions of several variables according to the following equation:

$$x = (x \mid x)x' + (x \mid \theta)\theta' + (x \mid y)y' + (x \mid \phi)\phi' + (x \mid \delta p)\delta p' \tag{4.1}$$

$$y = (y \mid x)x' + (y \mid \theta)\theta' + (y \mid y)y' + (y \mid \phi)\phi' + (y \mid \delta p)\delta p' \tag{4.2}$$

where the prime refers to the initial values of these variables. The values of x' and y' are close to zero at the entrance of the separator, so that equations 4.1 and 4.2 turns to be:

$$x = (x \mid \theta)\theta' + (x \mid \phi)\phi' + (x \mid \delta p)\delta p' \tag{4.3}$$

$$y = (y \mid \theta)\theta' + (y \mid \phi)\phi' + (y \mid \delta p)\delta p' \tag{4.4}$$

Since a large value of θ' and ϕ' leads to an increment of x and y, the angular acceptance of the separator can be determined by checking the maximum angles θ' and ϕ' of the nucleus in order to traverse the FRS. In addition, x and y also depend on the relative momentum deviation from the reference particle. Therefore, the angular acceptance will be a function of $\delta p'$. As already pointed out in section 1.3.1, $\delta p'$ is related to the transversal x-position of the nuclei at the second and fourth image planes through equations 1.12 and 1.13, where $\delta p'$ is different for each of them. Therefore, x_2 and x_4 are the global variables characterising the angular acceptance for any nucleus traversing the FRS.

In the following, we will describe how the map of the angular acceptance as a function of x_2 and x_4 can be calculated with our simulation code.

Firstly, the initial values of the coordinates defining the beam must be selected in order to calculate the transmission with the angular acceptance of the FRS uniformly populated. It will be explained later, how this calculation can be applied to estimate the angular acceptance of the separator:

- The transverse positions (x and y) at the entrance of the FRS (target) follow a uniform distribution of width ± 2.5 mm. This values are given by the emittance of the primary beam.

- The longitudinal coordinate (s) of all the nuclei constituting the beam is equal to zero.
- The initial angular distribution is uniform with a width equal to ± 30 mrad for both transverse angles θ and ϕ. This value is chosen in order to uniformly populate the full angular acceptance of the FRS.
- The angular acceptance must be calculated for any position at the second and fourth image planes. Hence, we performed the calculations at eleven different positions in the second and fourth image planes ($x_2 = 0, \pm 2, \pm 4, \pm 6, \pm 8$ and ± 10 and $x_4 = 0, \pm 2, \pm 4, \pm 6, \pm 8$ and ± 10). This leads to 121 calculated values which arise from all possible combinations between x_2 and x_4. In order to select the values of x_2 and x_4, a certain value of relative momentum deviation $\delta p'$ at the entrance and at the second image plane must be chosen for the particles traversing the FRS. This value is calculated with equations 1.12 and 1.13.

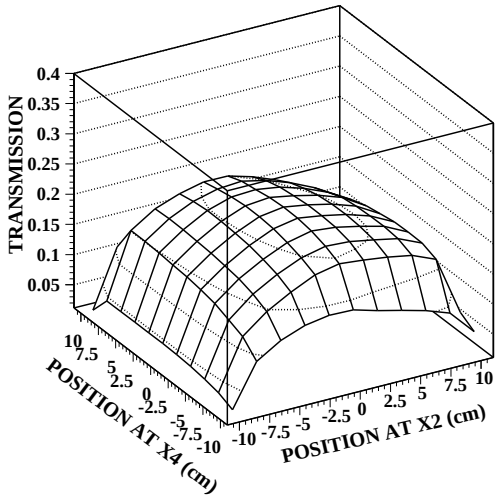

Figure 4.2: *Transmission of nuclei as a function of x_2 and x_4. The calculations were done assuming an uniform angular distribution covering ± 30 mrad.*

For each value of $\delta p'$, the transmission is calculated with the following formula:

$$T = \frac{N_{trans}}{N_0} \tag{4.5}$$

where N_0 is the number of incoming nuclei and N_{trans} is the number of nuclei arriving to the fourth image plane. Figure 4.2 shows a map of the transmission of nuclei as a function of their x_2 and x_4 positions, assuming an uniform angular distribution of the beam at the entrance of the FRS.

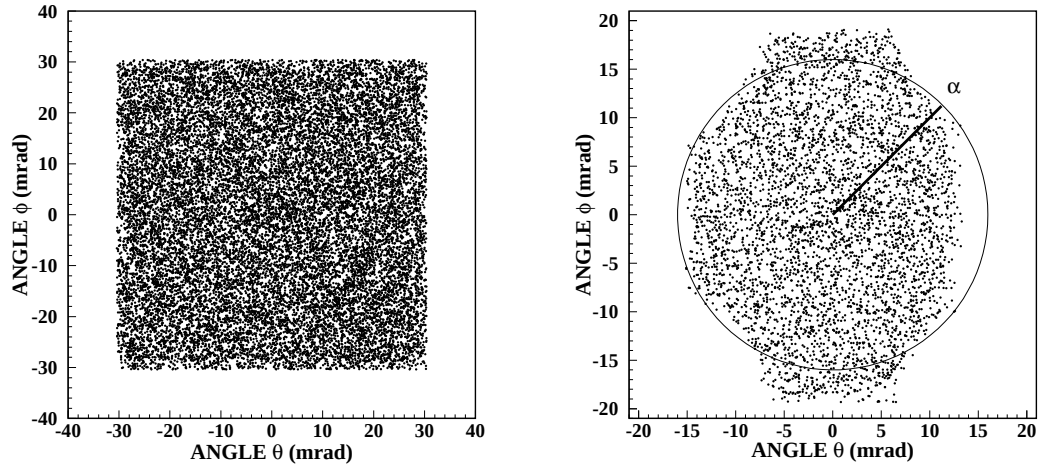

Figure 4.3: *Correlation between both transversal angles (θ, ϕ). Left: all the produced nuclei at the entrance of the FRS. Right: only transmitted nuclei until the fourth image plane for a beam centred at both image planes ($x_2 = x_4 = 0$).*

The left picture in figure 4.3 represents the initial angular distribution of nuclei at the entrance of the FRS. The right picture in the same figure shows the initial angular distribution of those nuclei transmitted through the FRS when the beam is centred at the second and fourth image planes ($x_2 = x_4 = 0$).

The ratio between the population of both pictures gives the transmission for this particular position (x_2, x_4). The angular acceptance for each position (x_2, x_4) can be determined if we approximate the shape of the angular distribution of the transmitted nuclei (right picture) by a circular distribution with an equivalent surface. The radius of this circular distribution gives the effective angular aperture of the separator for each position at the second and fourth image planes according to the following equation:

$$T(x_2, x_4) = \frac{\pi \alpha^2(x_2, x_4)}{S_0} \tag{4.6}$$

where $T(x_2, x_4)$ is the transmission shown in figure 4.2 and $\alpha(x_2, x_4)$ is the angular acceptance as a function of the position at the second and fourth image planes, and S_0 corresponds to the surface populated by the angular distribution of the incoming nuclei (in our case $S_0 = 60 \times 60$ mrad^2).

Finally, the angular acceptance $\alpha(x_2, x_4)$ can be calculated with equation 4.6. The results of this calculation are shown in figure 4.4. The figure shows a maximum acceptance of 15.9 mrad obtained when the beam traverses the FRS at the central position in both image planes. When the beam is shifted to the borders of these planes ($x_2 = x_4 = \pm$ 10 cm) the acceptance drops to values 70% lower.

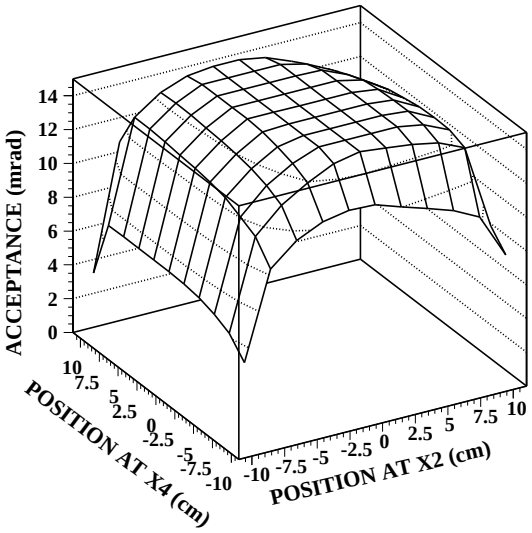

Figure 4.4: *Angular acceptance as a function of* x_2 *and* x_4.

4.3 Angular transmission

In the following, we will describe a method to calculate the transmission for any particle following a trajectory inside the FRS characterised by its positions at the second and fourth image planes. This method allows to determine analytically the transmission from the values of the angular acceptance shown in figure 4.4 and the mathematical description of the angular distribution of the reaction residues.

4.3.1 Fragmentation reactions

The transverse angles θ and ϕ of nuclei produced in fragmentation reactions follow a Gaussian distribution with widths given by equation 2.6. The intensity of fragments per solid angle can be described with the following equation:

$$\frac{dI}{d\Omega} = \frac{1}{2\pi\sigma(\theta)^2} exp\left(-\frac{\theta^2}{2\sigma(\theta)^2}\right) \tag{4.7}$$

where $\sigma(\theta)$ is the width of the angular distribution calculated from the Goldhaber or Morrisey equation [11, 12]. The intensity per angle is:

$$\frac{dI}{d\theta} \cong \frac{1}{\sigma(\theta)^2}\theta exp\left(-\frac{\theta^2}{2\sigma(\theta)^2}\right) \tag{4.8}$$

The transmission of nuclei produced in fragmentation reactions traversing the second and fourth image planes at positions given by x_2 and x_4 can be calculated by integrating the equation 4.8 over the range limited by the angular acceptance at this position:

$$T(x_2, x_4) = \int_0^{\alpha(x_2,x_4)} \frac{1}{\sigma(\theta)^2}\theta exp\left(-\frac{\theta^2}{2\sigma(\theta)^2}\right) \tag{4.9}$$

The result of this integration provides the following equation:

$$T(x_2, x_4) = 1 - exp\left(-\frac{\alpha^2(x_2, x_4)}{2\sigma(\theta)^2}\right) \tag{4.10}$$

This equations includes both the acceptances of the separator and the kinematics of the reaction ($\sigma(\theta)$). Once $\alpha(x_2, x_4)$ has been calculated by our program, we will know the transmission of any nuclei traversing the second and fourth image plane at different x-positions. Figure 4.5 shows the results of these calculations for three different values of $\sigma(\theta)$.

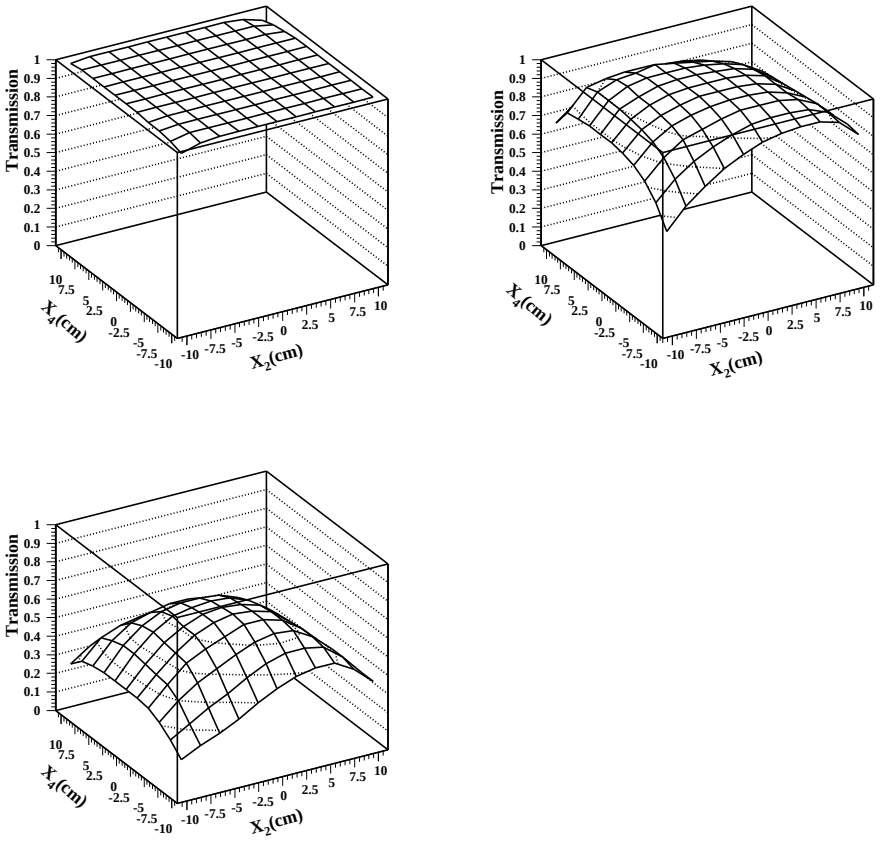

Figure 4.5: *Transmission as a function of x_2 and x_4 for three values of the angular aperture: $\sigma(\theta) = 2$ mrad (up-left), $\sigma(\theta) = 5$ mrad (up-right) and $\sigma(\theta) = 10$ mrad (down).*

4.3.2 Fission reactions

As already explained in chapter 2, for a given isotope produced in a fission reaction, a spherical momentum distribution assuming isotropic fragment emission is observed in the centre-of-mass frame of the two fission fragments. The Lorentz transformation into the laboratory frame leads to an ellipsoidal momentum distribution. In the space of momenta, the angular acceptance $\alpha(x_2, x_4)$ calculated for each position at the second and fourth image planes defines a cone which cuts the ellipsoid (figure 2.3). The ratio of the surface limited by this cone to the surface of the whole ellipsoid gives the transmission

of this isotope through the FRS [17]. This calculation can be simplified by transforming the angular acceptance from the laboratory frame into the centre-of-mass frame (appendix B). The Lorentz transformation splits the angular acceptance in two angles, one corresponding to the forward direction and the other to the backward direction (see figure 4.6).

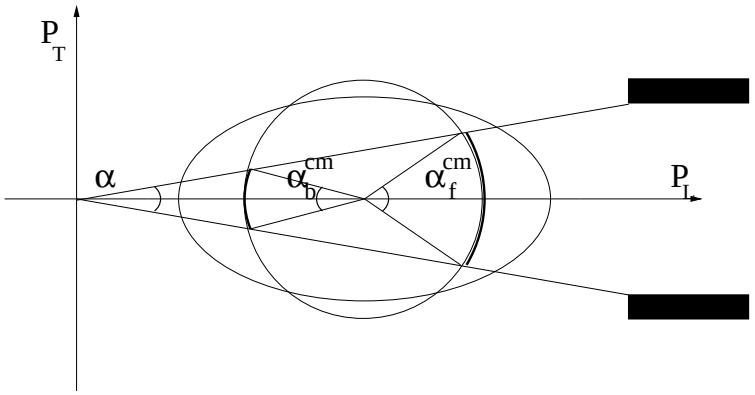

Figure 4.6: *Transformation of the momentum distribution from the laboratory frame to the centre-of-mass frame. P_L and P_T are the longitudinal and transverse momenta, respectively.*

The transmission of both forward- and backward-emitted fragments is determined by calculating the ratio of the surface limited either by the forward or by the backward angle to the surface of the whole spherical distribution:

$$T_f(x_2, x_4) = \frac{2\pi \int_0^{\alpha^f_{cm}(x_2,x_4)} \sin\theta d\theta}{4\pi} = \frac{1 - \cos(\alpha^f_{cm}(x_2, x_4))}{2} \tag{4.11}$$

and

$$T_b(x_2, x_4) = \frac{2\pi \int_0^{\alpha^b_{cm}(x_2,x_4)} \sin\theta d\theta}{4\pi} = \frac{1 - \cos(\alpha^b_{cm}(x_2, x_4))}{2} \tag{4.12}$$

where the index f and b refer to the forward and backward emission, and $\alpha_{cm}(x_2, x_4)$ is the angular acceptance in the centre-of-mass frame obtained from $\alpha(x_2, x_4)$ in the laboratory frame (figure 4.4). These angles are defined in the range $0 \leq \alpha_{cm} \leq \frac{\pi}{2}$.

4.4 Accuracy of the calculations

Before applying the results of the transmission calculations to the experimental measurements, one should estimate the precision of our method. There are several possible sources of error:

Shape and size of the inner tubes

The geometrical constraints of the FRS were simulated in our program by introducing a mathematical description of the shape and size of the inner tubes placed inside the different magnetic elements (see figure 4.1). This description was taken from the plans of the FRS. Nevertheless, there is a discrepancy of about 2 millimetres between the sizes given by the plans and those measured in the FRS. These measurements show that there is a deformation of the inner tubes. Since there are no more precise measurements of the sizes of the inner tubes, we tried to estimate the error of our simulation by calculating the angular acceptance with different values of the transversal dimensions of the inner tubes. The results showed that a modification of a few millimetres in these transverse dimensions leads to differences in the angular acceptance of $\sim 0.4\%$. Therefore, we can estimate an error in our calculations due to this effect of about $\sim 0.5\%$.

Transport of particles

As already pointed out, the transport of charged particles through a magnetic system is described by matrices (see appendix A). The coefficients of these matrices are calculated by expanding the equations of motion in a power series. In principle, our program must use matrices including higher-order terms in order to calculate the transmission characteristics of the FRS accurately. Nevertheless, one has to take into account that the time needed to simulate the transport of particles through the separator raises rapidly with increasing order of the terms included in the matrices. Our program uses matrices including terms up to third order. The simulation of the trajectories followed by the particles, performed with these matrices is sufficiently accurate to provide transmission values with a precisions better than 1%.

From these considerations we estimated a precision for our calculations of 2%. Furthermore, a dedicated experiment to determine the angular transmission in the FRS is planned to be done in order to check the accuracy of our calculations. In this experiment the total number of fission residues will be measured. The angular transmission will be evaluated by comparing the number of nuclei detected in this experiment with that obtained when the FRS was used to identify the produced isotopes.

4.5 Application of the calculated angular transmission into two experimental measurements

The method described in this chapter to evaluate the transmission of charged ions through the FRS was used to determine the total fission cross-section in two different reactions. The considered reactions are ^{197}Au(800 A MeV)+p and ^{208}Pb(1000 A MeV)+p. In these experiments, the produced fission residues were isotopically identified by the FRS as described in chapter 1. The kinematics of the reaction allowed to distinguish between fragmentation and fission reaction residues. A more detailed description of the experiments and data evaluation can be found in references [18, 19].

The fission residues were partially transmitted and identified due to the angular acceptance of the FRS. In order to determine the total fission cross-sections, we added up all the measured production yields for each isotope, which were corrected by the FRS transmission, evaluated using the method described in this chapter. The calculated values of the forward and backward transmission as a function of the velocity of the fission residues for the reaction ^{208}Pb(1000 A MeV)+p are shown in the left and right pictures of figure **??**. As expected the higher velocities have a lower transmission values than the lower ones.

Reaction	σ_f^{tot} (mbarn) (our results)	σ_f^{tot} (mbarn) (other results)
^{197}Au(800 A MeV) + p	72 ± 11	74.2 ± 7.4 [20]
^{208}Pb(1 A GeV) + p	159 ± 24	137 ± 14 [21]

Table 4.2: *Total fission cross sections of two different reactions measured in two different experiments.*

In table 4.2 we report the final total fission cross sections obtained for these two measurements. The present values are compared with those obtained in experiments dedicated to the measurement of the total fission cross-section for the same reactions. Our total fission cross sections are in good agreement (better than 15%) with the values measured in previous dedicated experiments. These results clearly show that we can be confident in our description of the transmission through the FRS. In fact, the accuracy of our

transmission evaluation is enough to be applied even for transmission losses as large as 80%.

Conclusion

Magnetic spectrometers provide high resolution measurements of the magnetic rigidity of charged particles or ions. This resolution provides a fully identification of the masses of heavy isotopes. Nevertheless, the limitation of the standard technologies does not allow to design these high resolution spectrometers with large acceptance in momentum and angle. In the case of zero-degree spectrometer the main limitation is the angular acceptance, specially when we use our spectrometer to identify isotopes produced in reactions leading to a large angular distribution of residues, as is the case of fission reactions.

In this work, we have performed a systematic investigation of the angular acceptance of the FRagment Separator (FRS) at GSI. In the first part of this work we presented two sets of experimental results which clearly illustrate this problem. In the first experiment we used a large acceptance experimental set-up to identify in charge the fission residues produced in the reaction ^{238}U(1 A GeV) + p. With this set up we were able to measure the full angular and momentum distributions of fission residues. In the second experiment we used the FRS to fully identify in mass and charge the fission residues produced in the same reaction. In this case the angular and momentum distributions were not fully transmitted through the FRS due to limited acceptance in angle and momentum. From the comparison of the angular and momentum distributions obtained in both experiments we were able to determine an average value of the transmission of the FRS for fission residues around 20%. Unfortunately, some technical limitations reported in chapter 3 did not allow a more precise determination of the transmission.

The second part of this work was devoted to a more theoretical approach intending to describe the transmission of particles through a magnetic spectrometer by using the ion optics formalism. This study allows us to develop a new method to estimate the angular transmission in magnetic spectrometers. Two factors determine the transmission of a charged particle: the acceptance of the spectrometer and the kinematics of the particle defining its trajectory. The main idea of the new method is to obtain a map of the acceptance of the

spectrometer as a function of global variables which characterised the trajectory of any particle. In our case we demonstrated that these global variables are the positions of the particles at the intermediate and final image planes of the spectrometer. Using this map of acceptance we can analytically estimate the transmission of any particle from the measurement of its positions at the two image planes and its velocity.

The main advantage of this method is that is very fast compared to the standard ion optics Monte-Carlo methods. Therefore this new method to estimate the angular transmission can be applied to experiments where a large amount a different isotopes are investigated. The results obtained in this work has already been used to correct the measured yields of fission residues in two different experiments dedicated to investigate the nature of the fission residues. The transmission corrections allowed to determine the production cross-sections of these fission residues and the sum of all of them gave the total fission cross section. The final results were checked by comparing the total fission cross sections with the ones obtained in dedicated experiments found in literature. The final results differs less than 15%. This good agreement indicate that we are able to estimate the angular transmission of the FRS with high accuracy, specially if we consider that this transmission is very low, typically 10%, and consequently the measured yields are corrected by large factors.

In addition, future experiments are planned to carefully check our calculations. These experiments will be performed with an improved large acceptance set-up. In this new experiments we will experimentally determine the angular transmission of the FRS as a function of the charge of the investigated nuclei.

Appendix A

Generalities on Ion Optic

This appendix is intended to provide a short introduction to the formalism describing the transport of charged particles in magnetic fields. Due to the analogies between ion-optic and geometrical optic, the formalism used when studying the behaviour of charged particles traversing a magnetic system is similar to that used in geometrical optic. A more detailed description of the Ion Optic can be found in reference [22].

This appendix is divided in three parts: in the first, we will explain the physical relation between magnetic and optic elements. In the second part we introduce the formalism and notation used to describe the trajectories of ions in magnetic fields. Finally, in the third part, some important concepts related to this topic will be defined.

A.1 Analogy between optical and magnetic systems

In order to justify the formalism used in ion-optic, we will establish the physical relations between magnetic elements and optic elements.

A.1.1 Prism versus Dipole

In geometric optic, a prism is the optic element which separates the different frequencies of a ray of white light. After the light crosses the prism, each ray with well defined frequency follows a trajectory with an angle depending on this frequency (figure A.1 left).

In the ion-optic framework, the equivalent magnetic element is a dipole. In this case, a charged particle traversing the magnet follows a trajectory which is deflected depending on its momentum or charge (figure A.1 right).

The curvature radius of the trajectory followed by the particle can be calculated with the next equation:

$$\rho = \frac{1}{B}\frac{p}{q} \tag{A.1}$$

where B is the magnetic field, p the momentum of the particle and q its charge.

Figure A.1 schematically illustrates the behaviour of a ray of light and a charged particle traversing a prism and a dipole magnet, respectively.

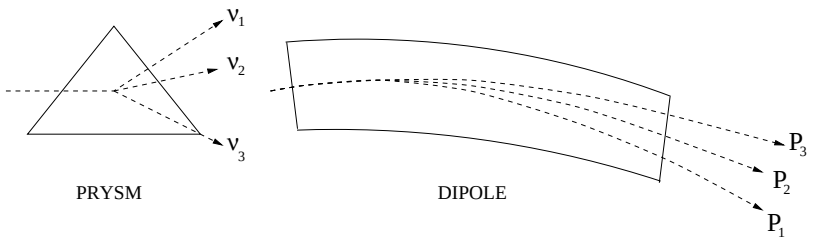

Figure A.1: *Left: White light (with a continuum spectrum of frequencies) enters into a prism. After crossing it, each frequency is split up in a different trajectory. Right: a bunch of charged particles with different momenta enters into a dipole. At the exit of the dipole, each particle with different momenta follows a different trajectory.*

A.1.2 Lenses versus Quadrupoles

In geometrical optic, the lenses can be classified in two kinds: lenses for focusing and lenses for defocusing. They are schematically depicted in figure A.2

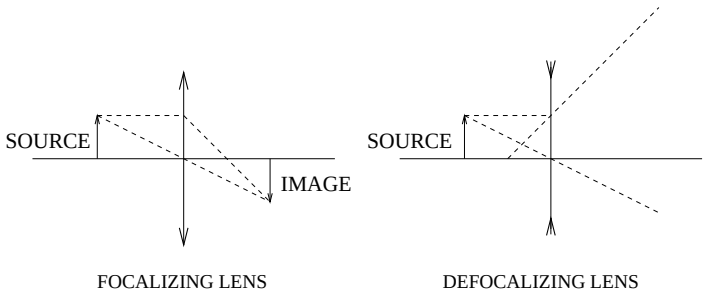

Figure A.2: *Left: focalisation of a ray of light performed by a lens. Right: defocalmisation of a ray of light.*

The magnetic element which "focuses" or "defocuses" the trajectory of the charged particle is the quadrupole. Figure A.3 shows the perpendicular section of the quadrupole respect to the trajectory followed by the beam of particles. The charged particle follows a trajectory depending on the direction of the field lines. This trajectory can be calculated by considering the Lorentz force:

$$\vec{F} = q \cdot \vec{v} \times \vec{B} \tag{A.2}$$

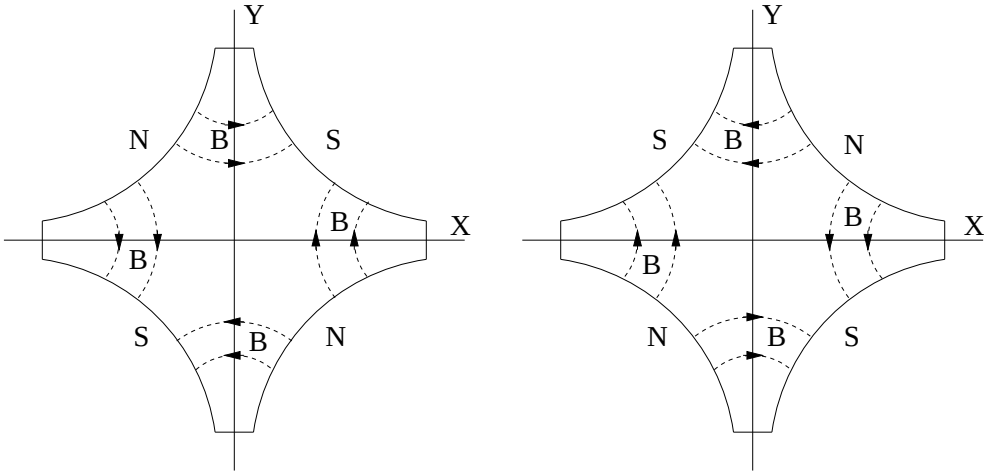

Figure A.3: *Cross section of two quadrupoles, one rotated* 90^o *respect to the other.*

Due to the structure of the quadrupoles, a particle focused in x-direction will be defocused in y-direction and vice-versa. Therefore, to achieve a complete focalization in both directions, it is necessary at least two quadrupoles rotated 90^o, one respect to the other. The intensity of the magnetic fields depends on the transversal distance from the position of the traversing particle to the symmetry axis of the quadrupole: it will vary from a minimum value equal to zero in the symmetry axis to a maximum value in the borders of the magnet. Figure A.4 illustrates the action of two quadrupoles focusing a charged particle.

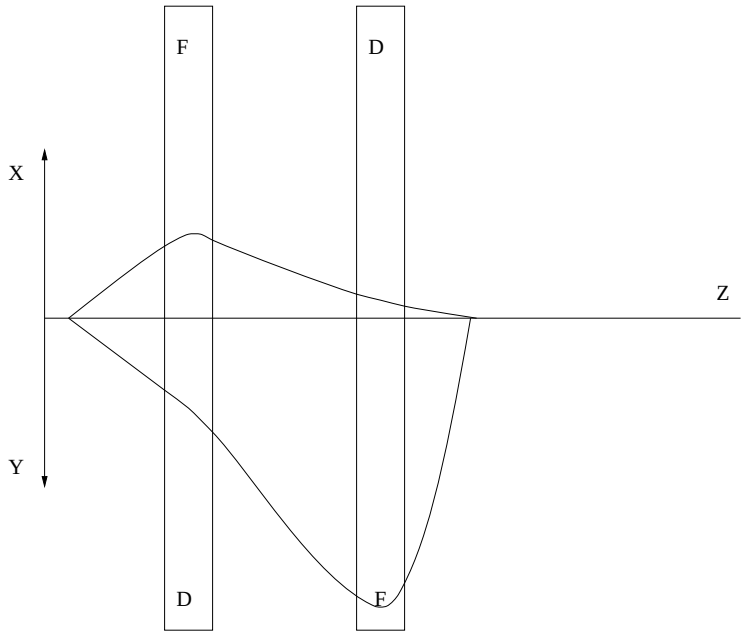

Figure A.4: *Focalization of the trajectory of a charged particle performed with two quadrupoles, one rotated* 90^o *respect to the other.* x *and* y *are the transversal coordinates of the particle respect to the symmetry axis of the magnets. The fist quadrupole focuses in* x *direction and defocuses in* y*, whereas the second quadrupole defocuses in* x *and focuses in* y*. The focusing power is proportional to the transversal distance to the symmetry axis (*z *axis).*

A.2 Ion-optical framework

A beam of particles can be represented by a set of points in the phase-space. In this space, each particle has three coordinates giving their position and three coordinates specifying the momentum.

From the region of phase-space populated by the beam, one can select a point to be the reference particle. The trajectory followed by this particle along the magnetic system is the central-trajectory and its momentum is the reference momentum p_c. The coordinates of the other particles are defined respect to those of the reference particle:

We will denote by s the distance along the central-trajectory. At any point of this trajectory we will define a vector $\vec{z}$ parallel to the reference momentum. Coordinates x and y are perpendicular to this vector and they specify the transversal distance to the central trajectory.

The momentum of each particle is defined by its three components p_x, p_y and p_t. In ion-optic formalism, another three different variables related with the momentum are used to describe the motion of charged particles in magnetic fields: they are the tangent of the transversal angles and the relative deviation from the reference momentum. The tangent is the ratio of transversal to longitudinal momentum:

$$\begin{aligned} \tan(\theta) &= \frac{p_x}{p_t} \\ \tan(\phi) &= \frac{p_y}{p_t} \end{aligned} \tag{A.3}$$

Since p_x and p_y are much smaller than p_t, we can approximate the angles by the value of their tangent:

$$\begin{aligned} \theta &\simeq \tan(\theta) \\ \phi &\simeq \tan(\phi) \end{aligned} \tag{A.4}$$

These coordinates are represented in figure A.5.

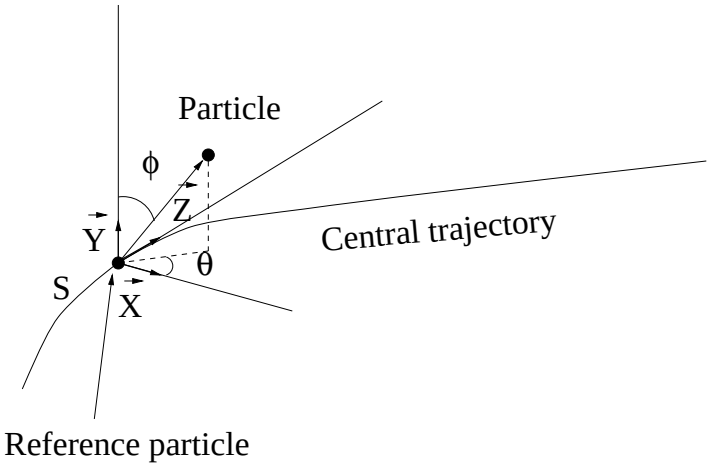

Figure A.5: *Reference frame and coordinates defining the state of a charged particle traversing a magnetic system.*

The fractional momentum deviation (δp) is defined by the following equation:

$$\delta p = \frac{p - p_c}{p_c} \tag{A.5}$$

where p_c is the reference momentum.

A.2.1 Matrix formalism

In the following, we will describe the mathematical formalism used when studying the behaviour of a charged particle in a magnetic system.

The trajectory followed by a charged particle along a magnetic element can be obtained solving its equations of motion for the different variables describing the trajectory:

$$\begin{aligned} m\frac{\partial x}{\partial s} &= F_x(x,\theta,y,\phi,\delta p) \\ m\frac{\partial \theta}{\partial s} &= F_\theta(x,\theta,y,\phi,\delta p) \\ m\frac{\partial y}{\partial s} &= F_y(x,\theta,y,\phi,\delta p) \\ m\frac{\partial \phi}{\partial s} &= F_\phi(x,\theta,y,\phi,\delta p) \end{aligned} \tag{A.6}$$

where m is the mass of the particle and F_x, F_θ, ... are complicated functions which can depend on the variables needed to define the state of the particle. The solution of these equations is also expressed by complicated functions:

$$\begin{aligned} x &= f_x(x',\theta',y',\phi',s',\delta p') \\ \theta &= f_\theta(x',\theta',y',\phi',s',\delta p') \\ y &= f_y(x',\theta',y',\phi',s',\delta p') \\ \phi &= f_\phi(x',\theta',y',\phi',s',\delta p') \end{aligned} \tag{A.7}$$

(A.8)

In order to simplify these solutions, we can expand them in a power series, including only lower order terms. The following equation shows this expansion up to first order terms:

$$\begin{aligned} x &= \frac{\partial x}{\partial x'}x' + \frac{\partial x}{\partial \theta'}\theta' + \frac{\partial x}{\partial y'}y' + \frac{\partial x}{\partial \phi'}\phi' + \frac{\partial x}{\partial s'}s' + \frac{\partial x}{\partial \delta p'}\delta p' \\ \theta &= \frac{\partial \theta}{\partial x'}x' + \frac{\partial \theta}{\partial \theta'}\theta' + \cdots \\ &\vdots \end{aligned} \tag{A.9}$$

where the prime refers to the initial values of the variables.

This simplification of the problem allows the description of the particle by a vector of six coordinates $\vec{X} = (x,\theta,y,\phi,s,\delta p)$, whereas the transport carried out by the magnetic element is condensed in a matrix:

$$\begin{pmatrix} (x \mid x) & (x \mid \theta) & (x \mid y) & (x \mid \phi) & (x \mid s) & (x \mid \delta p) \\ (\theta \mid x) & (\theta \mid \theta) & \cdots & \cdots & \cdots & (\theta \mid \delta p) \\ \vdots & \vdots & \vdots & \vdots & \vdots & \vdots \\ (\delta p \mid x) & (\delta p \mid \theta) & \cdots & \cdots & \cdots & (\delta p \mid \delta p) \end{pmatrix} \tag{A.10}$$

Here we have used the Brown notation [8], where $(x \mid x) = \partial x/\partial x'$, $(x \mid \theta) = \partial x/\partial \theta'$, an so on.

Therefore, each magnetic element can be described by a matrix, whereas the state of the traversing particles is given by a vector. The product of this vector to the matrixes describing the magnetic elements gives the evolution of the six coordinates specifying the state of the particle [8, 23]:

$$\begin{pmatrix} x \\ \theta \\ y \\ \phi \\ s \\ \delta p \end{pmatrix} = \begin{pmatrix} (x \mid x) & (x \mid \theta) & (x \mid y) & (x \mid \phi) & (x \mid s) & (x \mid p)) \\ (\theta \mid x) & (\theta \mid \theta) & \cdots & \cdots & \cdots & (\theta \mid p) \\ . & & & & & \\ . & & & & & \\ . & & & & & \\ . & & & & & \\ (\delta p \mid x) & (\delta p \mid \theta) & \cdots & \cdots & \cdots & (\delta p \mid p) \end{pmatrix} \cdot \begin{pmatrix} x' \\ \theta' \\ y' \\ \phi' \\ s' \\ \delta p' \end{pmatrix} \tag{A.11}$$

The equation described above includes only first order terms from the expansion of the solutions. This is a rough simplification which must be improved in order to get a more precise description of the trajectories followed by the particles. Therefore, higher order terms are often included in the matrix formalism. The calculation of such matrixes is a hard work which must be done by codes like GICO [16].

Nowadays, the matrix formalism is a very powerful tool used to design Monte-Carlo codes simulating the pass of charged particles through magnetic systems.

A.3 Important concepts used in ion-optic

A.3.1 Image plane

We define the image plane as the place where the transversal x and y positions of the particle do not depend on its transversal angles θ and ϕ, i.e.:

$$(x \mid \theta) \;=\; (x \mid \phi) = 0 \tag{A.12}$$

$$(y \mid \theta) \;=\; (y \mid \phi) = 0 \tag{A.13}$$

In most of the magnetic systems used in high and low energy physic such as spectrometers, accelerators or beam lines, the conditions to have an image plane can be achieved by using quadrupoles and sextupoles.

A.3.2 Magnification

Magnification is the variation in the magnitude of a coordinate of the particle, from one image plane to the next one. For instance, $(x \mid x)_{ij}$ is the magnification of the x-coordinate from the image plane i to the image plane j. Both dipoles and quadrupoles contribute to define the magnification of the system.

A.3.3 Dispersion

As mentioned in section A.1.1, a bending magnet deflects the trajectory of a charged particle depending on its charge and momentum. Two identical particles, following the same trajectory and with different momenta will have a different curvature radius inside a bending magnet, so that both trajectories will be separated after traversing the magnet. The transversal distance between the central-trajectory and the trajectory of a particle with δp=1% behind a bending magnet is called dispersion. In the Brown notation, the dispersion is defined as $(x \mid \delta p)$ and its value is expressed in $cm/\%$.

A.3.4 Achromatism

A magnetic system is achromatic when its dispersion is equal to zero, i.e. the deflection of particles does not depend on their momentum.

In order to express the conditions fulfilled by such a system in the matrix formalism, one has to consider the evolution of both the transversal x-coordinate and the relative momentum deviation of the traversing particle. The value of these two variables can be calculated with the following equation:

$$\begin{pmatrix} x_2 \\ \delta p_2 \end{pmatrix} = \begin{pmatrix} (x \mid x)_{02} & (x \mid \delta p)_{02} \\ 0 & 1 \end{pmatrix} \cdot \begin{pmatrix} x_0 \\ \delta p_0 \end{pmatrix} \tag{A.14}$$

where index 0 refers to the state of the particle at the entrance of the system and the index 2 to the state at the exit.

An achromatic system is always divided in two stages, both separated with a central image plane. The evolution of x and δp from the entrance of

the system to this central image plane are given by the next equation:

$$\begin{pmatrix} x_1 \\ \delta p_1 \end{pmatrix} = \begin{pmatrix} (x \mid x)_{01} & (x \mid \delta p)_{01} \\ 0 & 1 \end{pmatrix} \cdot \begin{pmatrix} x_0 \\ \delta p_0 \end{pmatrix} \tag{A.15}$$

and the same can be done from the central image plane to the end of the system:

$$\begin{pmatrix} x_2 \\ \delta p_2 \end{pmatrix} = \begin{pmatrix} (x \mid x)_{12} & (x \mid \delta p)_{12} \\ 0 & 1 \end{pmatrix} \cdot \begin{pmatrix} x_1 \\ \delta p_1 \end{pmatrix} \tag{A.16}$$

In this two equations, the index 1 refers to the central image plane.

Therefore, the matrix A.14 will be the product of the matrixes A.15 and A.16, so that:

$$\begin{pmatrix} (x \mid x)_{02} & (x \mid \delta p)_{02} \\ 0 & 1 \end{pmatrix} = \begin{pmatrix} (x \mid x)_{12} & (x \mid \delta p)_{12} \\ 0 & 1 \end{pmatrix} \cdot \begin{pmatrix} (x \mid x)_{01} & (x \mid \delta p)_{01} \\ 0 & 1 \end{pmatrix} . \tag{A.17}$$

From this equation we can calculate the dispersion of the whole system:

$$(x \mid \delta p)_{02} = (x \mid x)_{12} \cdot (x \mid \delta p)_{01} + (x \mid \delta p)_{12} \tag{A.18}$$

Since this dispersion must be equal to zero $(x \mid \delta p)_{02} = 0$, we can deduce the conditions that must satisfy each stage, in order to have an achromatic system:

$$(x \mid x)_{12} \cdot (x \mid \delta p)_{01} = -(x \mid \delta p)_{12} \tag{A.19}$$

Appendix B

Transformation of the angular acceptance into the centre-of-mass frame

The isotropy of the angular distribution of fission and fragmentation residues in the cetre-of-mass frame simplify considerably the evaluation of the transmission as was demonstrated in section 4.3.2. The calculated map of the angular acceptance in chapter 4 is done in the laboratory frame. To transform the acceptance from the laboratory frame we should consider the appropriate relativistic transformations as well as the kinematics of the reaction. In the first section of this appendix we will discuss the relativistic transformation of the angle from the laboratory to the centre-of-mass frame. In the second section we will show how we can obtain the kinematical parameters used in the frame transformation from the measured velocities.

B.1 Relativistic transformation

The value of the angular acceptance $\alpha_{lab}(x_2, x_4)$ for any trajectory inside the FRS (x_2, x_4)was determined in chapter 4 in the laboratory frame. The equivalent angle in the centre-of-mass frame can be calculated from the transversal and longitudinal velocities ($v_\perp$, $v_\parallel$) of the reaction residues in the centre-of-mass frame, by using the equations:

$$\alpha_{cm} = \frac{v_\perp}{v_\parallel} \tag{B.1}$$

The relation between α_{lab} and α_{cm} can be obtained taking into account the Lorentz transformation of the longitudinal and transversal velocities, as

shown in the following equation:

$$\alpha_{cm} = \frac{v_\perp}{\frac{v_\perp}{\gamma\alpha_{lab}} - V_{cm}} \tag{B.2}$$

where V_{cm} is the velocity of the centre-of-mass frame. Introducing the quadratic relation between the longitudinal and transversal velocities $\bar{v}^2 = v_\perp^2 + v_\parallel^2$ we obtain:

$$\alpha_{cm} = \frac{v_\perp}{\sqrt{\bar{v}^2 - v_\perp^2}} \tag{B.3}$$

From equations B.2 and B.3 we can calculate $v_\perp$ as:

$$v_\perp = \frac{b \pm \sqrt{b^2 - 4 \cdot a(V_{cm}^2 - \bar{v}^2)}}{2 \cdot a} \tag{B.4}$$

where

$$a = \frac{1}{\alpha_{lab}^2 \cdot \gamma^2} + 1 \tag{B.5}$$

$$b = \frac{2 \cdot V_{cm}}{\alpha_{lab} \cdot \gamma} \tag{B.6}$$

A similar procedure can be used to deduce the expression for the longitudinal velocity $v_\parallel$:

$$v_\parallel = \frac{b \pm \sqrt{b^2 - 4 \cdot a(V_{cm}^2 - \bar{v}^2)}}{2 \cdot a \cdot \alpha_{lab} \cdot \gamma} - V_{cm} \tag{B.7}$$

Equations B.1, B.4 and B.7 give us the transformation of the angular acceptance from the laboratory to the centre-of-mass frame. In this transformation, two kinematical parameters (V_{cm} and $\bar{v}$) are involved. In the next section we will discuss the method used to determine this two parameters.

B.2 Determination of V_{cm} amd $\bar{v}$

In this section we will discuss how to obtain the velocity of the residues in the centre-of-mass frame ($\bar{v}$) and the velocity of the centre-of-mass frame (V_{cm}) from the measured forward and backward velocities in the laboratory frame ($\bar{v}_{lab}^f$, $\bar{v}_{lab}^b$). Because we are interested in the velocities in the centre-of-mass frame, in figure B.1 we present an schematic representation of the measured and needed velocities in this frame. As you can see, the measured velocities in the centre-of-mass frame ($\bar{v}_{cm}^f$ and $\bar{v}_{cm}^b$) correspond to the mean value of the projection of the forward and backward velocity distribution along the longitudinal direction.

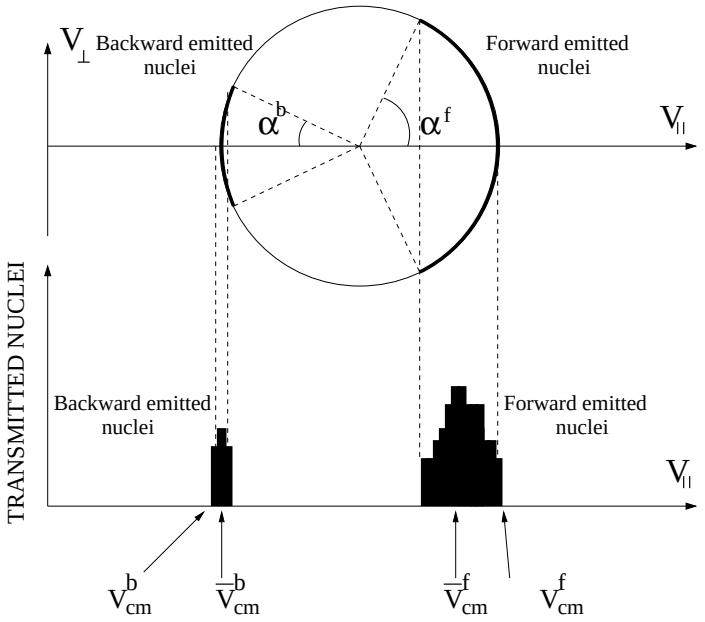

Figure B.1: *Up: Velocity distribution of a fission residue in the centre-of-mass frame. Down: velocity projection of the transmitted nuclei. The mean forward and backward velocities ($\bar{v}^f_{cm}$, $\bar{v}^b_{cm}$) do not coincide with the real velocities of the forward and backward emitted nuclei (v^f_{cm} and v^b_{cm}). These discrepancies raise with increasing the angular acceptances α^f_{cm} and α^b_{cm}.*

The relation between the measured velocities and the real ones ($\bar{v} = v^f_{cm} = v^b_{cm}$) is given by the angular acceptance α_{cm}, but in order to determine α_{cm} we should know $\bar{v}$. This problem can be solved using an iterative procedure. This procedure should also include the determination of the velocity of the centre-of-mass frame (V_{cm}) which is also unknown.

The starting point of the procedure is to consider the velocity of the primary beam in the centre of the target (v_{beam}) as the first reference frame. The measured velocities of the reaction residues ($\bar{v}^f_{lab}$, $\bar{v}^b_{lab}$) can be easily transformed to this reference frame giving ($\bar{v}^f_{beam}$, $\bar{v}^b_{beam}$). The mean value of these two velocities will give us a first guest for the velocity of the centre-of-mass frame in the beam frame.

$$V_{cm}(beam) = \frac{\bar{v}^f_{beam} + \bar{v}^b_{beam}}{2} \tag{B.8}$$

From $V_{cm}(beam)$ and the beam velocity v_{beam}, we can determine the velocity of the centre-of-mass in the laboratory frame V_{cm} with the Lorentz transfor-

mations:

$$V_{cm} = \frac{V_{cm}(beam) + v_{beam}}{1 + \frac{V_{cm}(beam) \cdot v_{beam}}{c2}} \tag{B.9}$$

With this last quantity we can determine the velocity of both fission fragments in the centre-of-mass frame (v^f_{cm}, v^b_{cm}) using the equations obtained in the previous section.

In the next iteraction step the quantities $\bar{v}^f_{beam}$, $\bar{v}^b_{beam}$ are increased. Because $\bar{v}^f_{beam}$ should increase faster than $\bar{v}^b_{beam}$ (see figure B.1) the increasing factor that we use is proportional to the respective transmissions in forward and backward directions given by α^f_{cm} and α^b_{cm}. The iteraction is repeated until $v^f_{cm} = v^b_{cm}$. At this point we obtain $\bar{v} = v^f_{cm} = v^b_{cm}$ and V_{cm}.

Bibliography

[1] H. Geissel et al., Nucl. Instr. and Meth. B70 (1992) 286-297

[2] The European Spallation Source Study, vol III, The ESS Technical Study, report ESS-96-53-M, 1996.

[3] C.D. Bowman et al., Nucl. Instr. and Meth. A320 (1992) 226.

[4] C. Rubbia et al., Report No. CERN/AT/95-44(ET),1995

[5] Isao Tanihata. Production and Use of Radioactive Beams. Experimental Techniques in Nuclear Physics, ed. by Dorin N. Poenaru and Walter Greiner. -Berlin; New York: de Gruyter,1997

[6] Gottfried M*ü*nzenberg. In-Flight Separation of Heavy Ion Beams. Experimental Techniques in Nuclear Physics, ed. by Dorin N. Poenaru and Walter Greiner.-Berlin; New York: de Gruyter,1997

[7] K.H. Schmidt, E. Hanelt, H. Geissel, G. M*ü*nzenberg and J.P. Dufour., Nucl. Instr. and Meth. A260 (1987) 287-303.

[8] K.L. Brown, SLAC-Report No 91, Stanford (1970).

[9] B. Voss, Nucl. Instr. and Meth. A364 (1995) 150.

[10] M. Pf*ü*tzner, B. Voss, H.-G. Clerc, H. Geissel, G. M*ü*nzenberg, F. Nickel, K.-H. Schmidt, M. Steiner, K. S*ü*mmerer and D.J. Vieira., Sci. Rep. GSI-91-1 (1991) 288.

[11] A.S. Goldhaber, Phys. Lett. B53 (1974) 306.

[12] D.J. Morrisey, Phys. Rev. C39 (1989) 460.

[13] B.D. Wilkins, E.P. Steinberg, R.R. Chasman., Phys. Rev. C14 (1976) 1832.

[14] K.H. Schmidt et al., Accepted for publication in Nucl. Phys.A. GSI-Preprint-99-30

[15] N. Iwasa, H. Geissel, G. M*ü*nzenberg, C. Scheidenberger, Th. Schwab, H. Wollnik., Nucl. Instr. and Meth. B126 (1997) 284-289.

[16] H. Wollnik, Manual for GICO (University of Gieβen, 1990).

[17] P. Armbruster et al., Z.Phys. A355, (1996) 191-201.

[18] J. Benlliure et al., Proc. of the Fourth International Conference Dynamical Aspects of Nuclear Fission, Casta Pappiernicka, Slovak Republic. October 1998

[19] W. Wlazlo et al., Proc. of the Third International Conference on Accelerator Driven Transmutation Technologies and Applications, Praha, Czech Republic. June 1999

[20] A.V. Prokofiev, Proc. of the Third International Conference on Accelerator Driven Transmutation Technologies and Applications, Praha, Czech Republic. June 1999

[21] L.A. Vaishnene et al., Z.Phys. A302, (1981) 143

[22] David C. Carey. The Optics of the Charged Particle Beams. Harwood Academic Publishers; Switzerland, 1987.

[23] S. Penner, Rev. Sci. Instr. 32 (1961) 150.